Bounds on Phase, Frequency, and Timing Synchronization in Fully Digital Receivers with 1-bit Quantization and Oversampling

Martin Schlüter, Meik Dörpinghaus, and Gerhard P. Fettweis
Vodafone Chair Mobile Communications Systems, SFB 912 HAEC,
Technische Universität Dresden, Dresden, Germany,
{martin.schlueter, meik.doerpinghaus, gerhard.fettweis}@tu-dresden.de

***Abstract*—Digital receivers based on 1-bit quantization and oversampling w.r.t. the transmit signal bandwidth promise lower energy consumption. However, since 1-bit quantization is a highly non-linear operation, standard receiver algorithms cannot be applied.**

Thus, we derive performance bounds for phase, timing, and frequency estimation in order to gain a deeper insight into the impact of 1-bit quantization and oversampling. We identify uniform phase and sample dithering as crucial to combat the effect of the non-linearity introduced by 1-bit quantization.

Since oversampling results in noise correlation, a closed form of the likelihood function is not available. Thus, we study a system model with white noise by adapting the receive filter bandwidth to the sampling rate. Considering the aforementioned dithering, we obtain very tight closed form lower bounds on the Cramér–Rao lower bound (CRLB) in the large sample regime. We show that with uniform phase and sample dithering, all large sample properties of the CRLB of the unquantized receiver are preserved under 1-bit quantization, except for an signal-to-noise ratio (SNR) dependent performance loss that can be decreased by oversampling. Numerical computations show that the properties of the CRLB for white noise still hold for colored noise except that the performance loss due to 1-bit quantization is reduced.

I. Introduction

With the increasing demand for faster communication systems, soon data rates in the terabit per second regime are required. It has recently been understood that analog-to-digital conversion forms a bottleneck at the receiver w.r.t. the power consumption. This motivates interest in low-resolution analog-to-digital converters (ADCs). The extreme case of 1-bit quantization is particularly interesting at very high datarates since for sampling frequencies beyond 100 MHz the energy per conversion step begins to increase linearly with the frequency, while for smaller sampling rates the energy per conversion step is independent of the sampling rate [1], [2]. Moreover, 1-bit quantization is advantageous as it is simple to realize since it requires no automatic gain control and no highly linear analog signal processing. In order to account for the information lost due to 1-bit amplitude resolution, we consider temporal oversampling.

Using numerical methods to compute the achievable rate, it was shown in [3], [4] that when using suitable modulation schemes and sequence design, oversampling can increase the achievable rate beyond 1 bit/s/Hz per real dimension. Moreover, a lower bound on the achievable rate of the continuous time (i.e., infinite oversampling) additive white Gaussian noise (AWGN) channel with 1-bit output quantization and strict bandlimitation was derived in [5], which confirmed the numerical results from [3]. Furthermore, [6] extended this approach to the downlink of massive multiple-input multiple-output (MIMO) systems in the Internet of things (IoT) context.

In general, 1-bit quantization has received significant attention in the context of massive MIMO, however, the literature on temporal oversampling is limited. It could be shown in [7] and [8] that oversampling w.r.t. the signaling rate improves the system performance, i.e., there is a trade off between the number of antennas and the oversampling factor when a particular system performance must be achieved. Moreover, it was demonstrated in [9] that temporal oversampling yields the same performance as spatial oversampling at reduced hardware complexity in 1-bit quantized wideband large-scale antenna systems.

However, all aforementioned papers assume perfect synchronization. For millimeter-wave (mmWave) MIMO orthogonal frequency-division multiplexing (OFDM) systems with low resolution ADCs frame timing and frequency synchronization has been considered in [10] and [11], while frame timing and frequency synchronization with 1-bit digital-to-analog converters (DACs) at the base station has been investigated in [12]. In [13] the joint synchronization of phase and frequency in a quadrature phase-shift keying (QPSK) and Nyquist rate based communication system with coarse phase quantization and perfect timing was considered and a bit error rate (BER) performance close to perfect synchronization could be achieved. Moreover, in [14] we considered a communication system based on run-length limited sequences and faster than Nyquist signaling with 1-bit quantization at the receiver, as proposed in [4], and showed that a known symbol timing offset can be compensated simply by oversampling w.r.t. the symbol rate. Furthermore, least squares estimation of the phase was considered in [15], where it was shown that oversampling

This work is supported by the Deutsche Forschungsgemeinschaft (DFG, German Research Foundation) in the Collaborative Research Center "Highly Adaptive Energy-Efficient Computing", SFB 912, HAEC, Project-ID 164481002. Moreover, this work has partly been presented at the IEEE International Communications Conference 2019 in Shanghai.

The authors are with the Vodafone Chair Mobile Communications Systems, SFB 912 HAEC, Technische Universität Dresden, 01062 Dresden, Germany.

This is a corrected versions where an error in (105) has been corrected.

improves the performance.

Nonetheless, a full investigation on joint timing, phase, and frequency synchronization has not been conducted yet. In order to understand the problem under 1-bit quantization, a first step is to analyze the fundamental limits of the channel parameter estimation, which are determined by the Fisher information (FI) and the Cramér–Rao lower bound (CRLB). Unfortunately, oversampling w.r.t. signal bandwidth results in noise correlation and it is a mathematically open problem to find an analytical description for the likelihood function of system models with colored Gaussian noise and 1-bit quantization, since there is no analytical description of the orthant probabilities [16, Chapter 2]. Thus, a lower bound on the FI was derived that requires only the first and second order moments [17]. This lower bound on the FI gives an upper bound on the CRLB, i.e., it indicates the performance an efficient estimator should at least achieve. Utilizing this bound, it could be shown for various estimation problems that oversampling improves the performance, e.g., for time-of-arrival estimation [18] or phase estimation [19].

Unfortunately, this bound can only be computed numerically and is thus not well suited for the purpose of understanding the effect of 1-bit quantization on the channel parameter estimation. Hence, we will consider white noise by adapting the receive filter bandwidth to the sampling frequency. Based on the example of phase estimation, it was shown in [19] that this method is inferior to considering colored noise. This is due to the fact that increasing the receive filter bandwidth increases the noise power, and thus decreases the signal-to-noise ratio (SNR). Hence, with increasing oversampling rate for white noise the performance loss compared to the unquantized case converges to the low SNR limit, where the FI of the 1-bit quantized signal is $\frac{2}{\pi}$ times smaller than the FI of the unquantized signal [20]. If the receive filter bandwidth is fixed to the bandwidth of the transmit signal, the noise is temporally correlated and oversampling can decrease the performance loss i.e., the loss factor becomes larger [18], [19]. However, considering white noise allows for an analytical treatment, and we will show numerically that the general behavior of the CRLB is similar under white and colored noise, the only difference is a reduced performance loss in case of colored noise. We already made a first step in [21], where we obtained very tight low and high SNR bounds on the CRLB of phase and frequency estimation assuming a known timing shift. Here we consider the more general case of an unknown timing shift.

Our contributions are summarized as follows.

- We analyze the FI of joint phase, timing, and frequency estimation of the 1-bit quantized receiver and observe that it is highly dependent on the phase of the signal. Thus, we propose to apply uniform phase dithering, which can be obtained in practice by sampling at an intermediate frequency (IF) that is irrational when normalized on the sampling rate. Due to the law of large numbers, this will average out the phase dependency for large observation intervals.
- For a general signal $\mathbf{s}(\boldsymbol{\theta})$, where $\boldsymbol{\theta}$ is the unknown parameter vector, we give a very tight approximation for the FI such that the effect of the non-linearity due to 1-bit quantization is represented by a Gaussian function. Subsequently, we derive a closed form solution of the FI if uniform phase dithering is applied.
- We apply the FI for uniform phase dithering to the estimation of phase, timing, and frequency of a linearly modulated signal and observe that the estimation of the timing parameter requires additional dithering in the sampling. This dithering can be obtained by ensuring that the oversampling factor is an irrational number w.r.t. the symbol rate. Moreover, since we apply random dithering that is independent of the signal, the receiver requires no feedback from the digital to the analog part.
- Based on Jensen's inequality we derive a very tight lower bound on the CRLB of phase and frequency, considering dithering in phase and sampling. Moreover, numerical evaluations for raised cosine and root raised cosine pulses demonstrate that the same bounding technique can be applied to the CRLB of the timing parameter. This bound is equal to the CRLB of the unquantized receiver up to a loss factor that depends on the SNR and the oversampling factor. I.e., if phase and sample dithering is applied, all large sample properties of the CRLB of the unquantized receiver are preserved under 1-bit quantization, e.g., the phase estimation performance is independent of the transmit pulse form.
- Finally we compare the results for white noise with the numerically computed CRLB upper bound for colored noise. We observe that the properties proven for white noise also hold for colored noise, but the colored noise case yields a better performance.

An alternative design for a receiver employing 1-bit quantization was presented in [22]. The authors proposed an architecture that can be interpreted as oversampling with 1-bit quantization and varying thresholds. Simply put, we propose low IF sampling with an oversampling factor that is irrational w.r.t. the symbol rate and the authors of [22] propose amplitude dithering and oversampling with an oversampling factor that is an integer. The implementational advantage of our design is the fact that our receiver does not require an automatic gain control (AGC), a simple limiting amplifier in front of the 1-bit ADC suffices. A 1-bit quantizer with varying thresholds inherently needs an AGC as the amplitude of the input signal has to lie within the range of the varying thresholds.

Phase dithering was also considered in [13]. However, instead of uniform phase dithering a feedback based dithering was applied, where the feedback signal is computed based on the previous samples, which effectively results in a digitally controlled phase-locked loop (PLL). This leads to a better performance than uniform phase dithering, but increases the hardware complexity compared to simple low IF sampling. However, in terms of phase, frequency, and timing estimation we will show that uniform phase dithering can achieve the performance of optimal feedback based dithering if the oversampling factor is large enough. In this regard, higher SNR requires a larger oversampling factor to achieve this.

The remainder of this paper is organized as follows. In Section II we introduce the system model and in Section III we review some important properties of the unquantized

receiver and its CRLB. Subsequently, we analyze the FI of the 1-bit quantized receiver for white noise and propose uniform phase dithering to combat the phase dependency in Section IV. Moreover, we review the CRLB upper bound for colored noise. In Section V we derive a closed form solution for the FI of a general signal model $\mathbf{s}(\boldsymbol{\theta})$ if uniform phase dithering is applied and then apply this solution to the signal model from Section II. Based on Jensen's inequality we derive a very tight lower bound for the CRLB of phase, timing, and frequency and give approximations for low and high SNR. Finally, we assess the derived bounds and compare the results for white noise with the numerically obtained CRLB upper bound for colored noise in Section VI. Finally, we conclude our work in VII.

II. System Model

We consider the linearly modulated transmit signal

$$u(t) = \sum_{n=-(N/2)}^{(N/2)-1} a_n g\left(t - nT - \epsilon T\right). \tag{1}$$

The N symbols $\{a_n\}$ are chosen from an arbitrary signal constellation over the complex plane and $g(t)$ is the impulse response of the pulse shaping filter of single sided bandwidth $W_g = \frac{\alpha+1}{2T}$, where T is the symbol duration and $\alpha \in [0,1]$ is the roll-off factor. Moreover, the pulse $g(t)$ contains a deterministic but unknown time shift $\epsilon \in [-0.5, 0.5]$ w.r.t. the time reference of the receiver to express time shifts at the sub-symbol interval level. This signal is modulated onto the carrier frequency f_c, where it is disturbed by white Gaussian noise with power spectral density $N_0/2$. Furthermore, the channel introduces a deterministic but unknown phase rotation ϕ and frequency offset Ω. At the receiver the signal is demodulated and filtered with a rectangular receive filter of single sided bandwidth $W_r \geq W_g$. The receiver samples with a period of $T_s \leq \frac{1}{2W_r}$ and introduces a known phase dither φ_k such that the sampled receive signal is given by

$$r_k = s_k(\boldsymbol{\theta}) + \eta_k \tag{2}$$

with

$$s_k(\boldsymbol{\theta}) = \sum_{n=-(N/2)}^{(N/2)-1} a_n g\left(kT_s - nT - \epsilon T\right) e^{j(\Omega k T_s + \phi + \varphi_k)}, \tag{3}$$

where $\boldsymbol{\theta} = [\phi, \Omega, \epsilon]$ are the unknown parameters that shall be estimated and $\boldsymbol{\eta} = [\ldots, \eta_k, \eta_{k+1}, \ldots]^T$ is circularly-symmetric complex Gaussian noise with independent real and imaginary part and covariance matrix [23, Theorem 3]

$$\left[\mathbf{R}_{\boldsymbol{\eta}}\right]_{ij} = 2N_0 W_r \operatorname{sinc}\left(2W_r T_s \left|j - i\right|\right). \tag{4}$$

If we match the receive filter bandwidth to the sampling period, i.e., $W_r = 1/(2T_s)$, the noise is white with $\mathbf{R}_{\boldsymbol{\eta}} = (N_0/T_s)\mathbf{I} = \sigma^2\mathbf{I}$. In this case, the SNR is given by $\mathrm{SNR} = \frac{E_s/T}{N_0/T_s} = \frac{E_s}{N_0 M}$, where $E_s = \mathrm{E}\left[a_n^* a_n\right] \int |g(t)|^2 \, dt$ is the symbol energy and $M = \frac{T}{T_s}$ is the oversampling factor w.r.t. the symbol rate. Since the noise is circularly-symmetric, its density is not influenced by the phase dithering. In case of 1-bit quantization, the receiver only has access to

$$y_k = \operatorname{csign}(r_k) = \operatorname{sign}\left(\operatorname{Re}\{r_k\}\right) + j \cdot \operatorname{sign}\left(\operatorname{Im}\{r_k\}\right) \tag{5}$$

where the signum function $\operatorname{sign}(x) = 1$ if $x > 0$ and $\operatorname{sign}(x) = -1$ if $x \leq 0$, is applied elementwise in case of vectors. In the subsequent sections, we will denote $\mathbf{r} = [\ldots, r_k, r_{k+1}, \ldots]^T$ as the vector that contains the samples r_k. Other sample vectors are named accordingly. Moreover, we assume that $\{a_n\}$ is a random sequence of N independent identically distributed (i.i.d.) known symbols and that the phase dither realizations φ_k are known.

III. Digital Receiver without Quantization

Since the traditional unquantized receiver serves as a benchmark for the receiver based on 1-bit quantization and oversampling, we want to review some known facts on fully digital receivers where synchronization is done completely in the digital domain. At first we want to justify the choice of an ideal rectangular receive filter that is not realizable in practice. It was shown in [24] that the samples r_k are a sufficient statistic on the estimation of the channel parameters $\boldsymbol{\theta}$ as well as the transmitted symbols $\{a_n\}$ if $W_r = B$ and $T_s \leq \frac{1}{2W_r}$, where B is the bandwidth of the noiseless receive signal. Furthermore, [24] gave conditions on the analog receive filter and the sampling rate T_s such that the sufficient statistic property holds for a realizable filter, which basically is the requirement that the aliasing of the noise does not reach into the band of the useful part of the receive signal. This justifies our simplified assumptions of a rectangular receive filter.

Moreover, [24] and [25] have argued that the sampling rate T_s does not need to be matched to the symbol rate T, i.e., synchronization can be performed with samples r_k from a free running clock. I.e., the mixer and the sampler are free running oscillators at fixed frequencies, no phased lock loops are required. Note however, that a coarse carrier frequency adjustment is required in the intermediate frequency stages, since phase and timing recovery only work well for small frequency offsets. The residual frequency offset can also be synchronized in the digital domain.

After discussing a possible implementation of a fully digital receiver, we are interested in performance bounds on the estimation of the parameters $\boldsymbol{\theta}$. For $\boldsymbol{\theta} \in \mathbb{R}^L$ the FI of an observation vector $\mathbf{x}$ is defined as the positive semidefinite matrix

$$\left[\mathbf{F}_{\mathbf{x}}\right]_{\theta_i\theta_j} = \mathrm{E}_{\mathbf{x}|\boldsymbol{\theta}}\left[\left(\frac{\partial}{\partial\theta_i}\log\, p\left(\mathbf{x}|\boldsymbol{\theta}\right)\right)\left(\frac{\partial}{\partial\theta_j}\log\, p\left(\mathbf{x}|\boldsymbol{\theta}\right)\right)\right], \tag{6}$$

where $p(\mathbf{x}|\boldsymbol{\theta})$ is the likelihood function. For the unquantized observation vector $\mathbf{r}$ that is received in additive circularly-symmetric complex Gaussian noise, the FI matrix is given by

$$\left[\mathbf{F}_{\mathbf{r}}\right]_{\theta_i\theta_j} = 2\mathrm{Re}\left\{\frac{\partial \mathbf{s}^H}{\partial\theta_i}\mathbf{R}_{\boldsymbol{\eta}}^{-1}\frac{\partial \mathbf{s}}{\partial\theta_j}\right\}. \tag{7}$$

In favor of notational convenience, we dropped the argument $\boldsymbol{\theta}$ from $\mathbf{s}$. For any unbiased estimator $\hat{\boldsymbol{\theta}}(\mathbf{r})$, its covariance is lower-bounded by the CRLB

$$\mathrm{Cov}\left[\hat{\boldsymbol{\theta}}(\mathbf{r})\right] \geq \mathbf{F}_{\mathbf{r}}^{-1}, \tag{8}$$

where $\mathbf{A} \geq \mathbf{B}$ means that $\mathbf{A} - \mathbf{B}$ is positive semidefinite. Note that this bound requires the FI matrix to be invertible, i.e., it must be positive definite.

In case of white noise, i.e., $W_r = \frac{1}{2T_s}$, i.i.d. known symbols $\{a_n\}$, large N, a real valued pulse $g(t)$, and a symmetrical summation interval [26, Chapter 6.2], one obtains the fairly simple closed form solutions

$$[\mathbf{F_r}]_{\phi\phi} = \frac{2}{N_0/T_s}\sum_k |s_k|^2 \tag{9}$$

$$= 2N\frac{E_s}{N_0}, \tag{10}$$

$$[\mathbf{F_r}]_{\Omega\Omega} = \frac{2}{N_0/T_s}\sum_k k^2T_s^2\,|s_k|^2 \tag{11}$$

$$= 2\frac{E_s}{N_0}\left(\frac{(N^2-1)N}{12}T^2 + T^2N\epsilon^2 + N\frac{\int_{-\infty}^{\infty} t^2\,|g(t)|^2\,dt}{\int_{-\infty}^{\infty}|g(t)|^2\,dt} + 2N\epsilon T\frac{\int_{-\infty}^{\infty} t\,|g(t)|^2\,dt}{\int_{-\infty}^{\infty}|g(t)|^2\,dt}\right), \tag{12}$$

$$[\mathbf{F_r}]_{\epsilon\epsilon} = \frac{2}{N_0/T_s}\sum_k \frac{\partial s_k^*}{\partial\epsilon}\frac{\partial s_k}{\partial\epsilon} \tag{13}$$

$$= 2N\frac{E_s}{N_0}T^2 4\pi^2\frac{\int_{-\infty}^{\infty} f^2\,|G(f)|^2\,df}{\int_{-\infty}^{\infty}|G(f)|^2\,df}, \tag{14}$$

$$[\mathbf{F_r}]_{\phi\Omega} = \frac{2}{N_0/T_s}\sum_k kT_s\,|s_k|^2 \tag{15}$$

$$= 2N\frac{E_s}{N_0}\left(\epsilon T + \frac{\int_{-\infty}^{\infty} t\,|g(t)|^2\,dt}{\int_{-\infty}^{\infty}|g(t)|^2\,dt}\right), \tag{16}$$

and

$$[\mathbf{F_r}]_{\phi\epsilon} = [\mathbf{F_r}]_{\Omega\epsilon} = 0, \tag{17}$$

where $G(f)$ is the Fourier transform of $g(t)$. Thus, with

$$[\mathbf{F_r}] = \begin{bmatrix} [\mathbf{F_r}]_{\phi\phi} & [\mathbf{F_r}]_{\phi\Omega} & 0 \\ [\mathbf{F_r}]_{\Omega\phi} & [\mathbf{F_r}]_{\Omega\Omega} & 0 \\ 0 & 0 & [\mathbf{F_r}]_{\epsilon\epsilon} \end{bmatrix} \tag{18}$$

we obtain [26, Chapter 6.1]

$$\left[\mathbf{F_r^{-1}}\right]_{\phi\phi} = \frac{1}{[\mathbf{F_r}]_{\phi\phi} - [\mathbf{F_r}]_{\phi\Omega}^2/[\mathbf{F_r}]_{\Omega\Omega}} \tag{19}$$

$$= \left[2\frac{E_s}{N_0}\right]^{-1}\frac{1}{N}\frac{1}{1-O\left(N^{-2}\right)}, \tag{20}$$

$$\left[\mathbf{F_r^{-1}}\right]_{\Omega\Omega} = \frac{1}{[\mathbf{F_r}]_{\Omega\Omega} - [\mathbf{F_r}]_{\phi\Omega}^2/[\mathbf{F_r}]_{\phi\phi}} \tag{21}$$

$$= \left[2\frac{E_s}{N_0}\right]^{-1}\frac{12}{(N^2-1)NT^2}\frac{1}{1+O\left(N^{-2}\right)}, \tag{22}$$

and

$$\left[\mathbf{F_r^{-1}}\right]_{\epsilon\epsilon} = \frac{1}{[\mathbf{F_r}]_{\epsilon\epsilon}} \tag{23}$$

$$= \left[2\frac{E_s}{N_0}\right]^{-1}\frac{1}{N}\frac{1}{T^2 4\pi^2}\frac{\int_{-\infty}^{\infty}|G(f)|^2\,df}{\int_{-\infty}^{\infty} f^2\,|G(f)|^2\,df}. \tag{24}$$

Moreover, for large N, $\left[\mathbf{F_r^{-1}}\right]_{\phi\phi}$ and $\left[\mathbf{F_r^{-1}}\right]_{\Omega\Omega}$ can be approximated by

$$\left[\mathbf{F_r^{-1}}\right]_{\phi\phi} = \left[2\frac{E_s}{N_0}\right]^{-1}\frac{1}{N} \tag{25}$$

and

$$\left[\mathbf{F_r^{-1}}\right]_{\Omega\Omega} = \left[2\frac{E_s}{N_0}\right]^{-1}\frac{12}{(N^2-1)NT^2}. \tag{26}$$

Thus (25) is equal to $[\mathbf{F_r}]^{-1}_{\phi\phi}$. Furthermore, one can verify that

$$[\mathbf{F_r}]^{-1}_{\Omega\Omega} = \left[2\frac{E_s}{N_0}\right]^{-1}\frac{12}{(N^2-1)NT^2}\frac{1}{1+O\left(N^{-2}\right)} \tag{27}$$

such that $\left[\mathbf{F_r^{-1}}\right]_{\Omega\Omega}$ equals $[\mathbf{F_r}]^{-1}_{\Omega\Omega}$ for large N. Thus, the cross-terms of the FI matrix can be neglected for large N such that

$$\left[\mathbf{F_r^{-1}}\right]_{\theta_i\theta_i} = [\mathbf{F_r}]^{-1}_{\theta_i\theta_i}. \tag{28}$$

Moreover, the CRLB is independent of the sampling rate, as long as the conditions given on the analog receive filter and the sampling rate T_s given in [24] are fulfilled. Even if we do not adapt the receive filter bandwidth to the oversampling factor such that the noise is colored, i.e., we chose the minimum possible receive filter bandwidth that fulfills the conditions in [24], the CRLB does not improve [26, Chapter 6.1].

IV. Digital Receiver with 1-bit Quantization

In this section we want to study the FI in case of 1-bit quantization. We will review the FI in the case of white noise and subsequently argue that phase dithering is crucial to reduce the effect of the non-linearity introduced by 1-bit quantization. Finally we will discuss how an upper bound on the CRLB can be obtained in case the noise is colored.

A. White Noise

From [19], [20] we know that the FI in case white Gaussian noise is given by

$$\left[\mathbf{F_y}\right]_{\theta_i\theta_j} = \frac{1}{\pi\sigma^2}\sum_k\left(\frac{e^{-\frac{(\mathrm{Re}\{s_k\})^2}{\sigma^2/2}}\frac{\partial}{\partial\theta_i}\mathrm{Re}\{s_k\}\,\frac{\partial}{\partial\theta_j}\mathrm{Re}\{s_k\}}{Q\left(\frac{\mathrm{Re}\{s_k\}}{\sigma/\sqrt{2}}\right)Q\left(-\frac{\mathrm{Re}\{s_k\}}{\sigma/\sqrt{2}}\right)} + \frac{e^{-\frac{(\mathrm{Im}\{s_k\})^2}{\sigma^2/2}}\frac{\partial}{\partial\theta_i}\mathrm{Im}\{s_k\}\,\frac{\partial}{\partial\theta_j}\mathrm{Im}\{s_k\}}{Q\left(\frac{\mathrm{Im}\{s_k\}}{\sigma/\sqrt{2}}\right)Q\left(-\frac{\mathrm{Im}\{s_k\}}{\sigma/\sqrt{2}}\right)}\right) \tag{29}$$

$$= \frac{1}{\pi\sigma^2}\sum_k\left(B\left(\frac{\mathrm{Re}\{s_k\}}{\sigma/\sqrt{2}}\right)\frac{\partial}{\partial\theta_i}\mathrm{Re}\{s_k\}\,\frac{\partial}{\partial\theta_j}\mathrm{Re}\{s_k\} + B\left(\frac{\mathrm{Im}\{s_k\}}{\sigma/\sqrt{2}}\right)\frac{\partial}{\partial\theta_i}\mathrm{Im}\{s_k\}\,\frac{\partial}{\partial\theta_j}\mathrm{Im}\{s_k\}\right), \tag{30}$$

where $B(\cdot)$ was introduced to simplify notation. Furthermore, under the white noise assumption, we can rewrite the FI of the unquantized receiver as

$$[\mathbf{F}_\mathbf{r}]_{\theta_i\theta_j} = 2\mathrm{Re}\left\{\frac{\partial \mathbf{s}^H}{\partial\theta_i}\mathbf{R}_\eta^{-1}\frac{\partial \mathbf{s}}{\partial\theta_j}\right\} \tag{31}$$

$$= \frac{2}{\sigma^2}\sum_k \mathrm{Re}\left\{\frac{\partial}{\partial\theta_i}s_k^*\frac{\partial}{\partial\theta_j}s_k\right\} \tag{32}$$

$$= \frac{2}{\sigma^2}\sum_k\left(\frac{\partial}{\partial\theta_i}\mathrm{Re}\{s_k\}\frac{\partial}{\partial\theta_j}\mathrm{Re}\{s_k\} + \frac{\partial}{\partial\theta_i}\mathrm{Im}\{s_k\}\frac{\partial}{\partial\theta_j}\mathrm{Im}\{s_k\}\right). \tag{33}$$

Comparing (33) with (30) we observe that the only difference is a multiplicative factor of $\frac{1}{2\pi}$ and the scaling by $B(\cdot)$. This non-linear scaling due to 1-bit quantization renders the FI highly dependent on the phase rotation, as we will see in the subsequent section. For the usual case that $\mathbf{F}_\mathbf{y}$ and $\mathbf{F}_\mathbf{r}$ are positive definite, we will prove in Appendix A that

$$\mathbf{F}_\mathbf{y} \preceq \frac{2}{\pi}\mathbf{F}_\mathbf{r}. \tag{34}$$

Equality will hold for $\sigma \to \infty$, a fact well known [20]. Moreover, from [27, Corollary 7.7.4 (a)] it follows directly that

$$\mathbf{F}_\mathbf{y}^{-1} \succeq \frac{\pi}{2}\mathbf{F}_\mathbf{r}^{-1}. \tag{35}$$

B. Phase Dithering

We now want to study the FI of phase, timing, and frequency and argue that phase dithering is crucial to reduce the effect of the non-linearity introduced by 1-bit quantization. In [13] and [19] the problem of phase estimation with QPSK signaling and 1-bit quantization was studied. It was found that the parameter estimation accuracy is highly dependent on the phase of the receive signal. If the samples r_k are close to the decision boundary in the complex plane, the FI is high, but when the samples lie within the middle of a quadrant the FI is low. The higher the SNR, the more pronounced is this effect. This is intuitive, since in the noiseless case for every sample r_k the same 1-bit quantized measurement y_k would be observed, which results in a poor estimation performance. In Fig. 1 this effect is illustrated by the loss function

$$\chi(\phi) = \frac{\left[\mathbf{F}_\mathbf{r}^{-1}\right]_{\phi\phi}}{\left[\mathbf{F}_\mathbf{y}^{-1}\right]_{\phi\phi}} \tag{36}$$

for the observation of a single QPSK symbol under the assumption that ϵ and Ω are known. We see that the phase dependency is high for high SNR and vanishes for low SNR, where the loss factor approaches $\frac{2}{\pi}$. Note that, $\chi(\phi)$ cannot be larger than $\frac{2}{\pi}$, as stated in (35).

As a second example we want to examine the cross term $\left[\mathbf{F}_\mathbf{y}^{-1}\right]_{\phi\epsilon}$ under the assumption that Ω is known, i.e., the FI matrix is reduced to a 2x2 matrix. For the unquantized receiver, the cross term $[\mathbf{F}_\mathbf{r}]_{\phi\epsilon}$ vanishes for large N if $g(t)$ is real valued. Thus, $\mathbf{F}_\mathbf{r}$ is a diagonal matrix and $\left[\mathbf{F}_\mathbf{r}^{-1}\right]_{\phi\epsilon}$ vanishes as well. However, this is does not happen in case of 1-bit quantization. Since $\mathbf{F}_\mathbf{y}^{-1}$ describes an asymptotically ($N \to \infty$) achievable

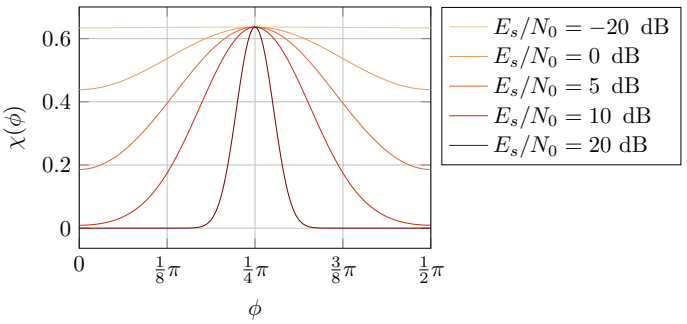

Fig. 1: FI ratio $\chi(\phi)$ of a single QPSK symbol (i.e., $N = 1$) with $T_s = T$, $\varphi_k = 0$ and ϵ and Ω are known to be zero. Since $\left[\mathbf{F}_\mathbf{y}\right]_{\phi\phi}$ is periodic with $\frac{\pi}{2}$, we restrict the interval to $\phi \in \left[0, \frac{\pi}{2}\right]$.

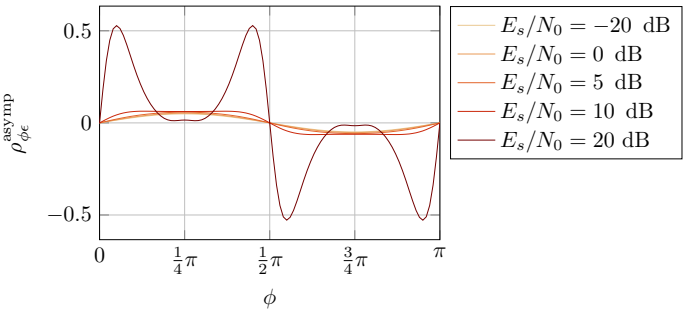

Fig. 2: Asymptotic achievable correlation between ϕ and ϵ, for $N = 100$, $M = 2$, root raised cosine pulses $g(t)$ with $\alpha = 0.2$, $\epsilon = 0$, $\varphi_k = 0$, and $T = 1$, obtained by Monte Carlo simulation over 1000000 random sequences $\{a_n\}$. Moreover, Ω is known to be zero. Due to periodicity with π, we restricted the interval to $\phi \in [0, \pi]$.

covariance matrix of $\hat{\boldsymbol{\theta}}$ [28], we define the asymptotically achievable correlation coefficient

$$\rho_{\phi\epsilon}^{\mathrm{asymp}} = \frac{\left[\mathbf{F}_\mathbf{y}^{-1}\right]_{\phi\epsilon}}{\sqrt{\left[\mathbf{F}_\mathbf{y}^{-1}\right]_{\phi\phi}\left[\mathbf{F}_\mathbf{y}^{-1}\right]_{\epsilon\epsilon}}} \tag{37}$$

that is plotted in Fig. 2. We observe that the correlation depends on ϕ, where the dependency increases with increasing SNR.

To overcome this phase dependency, phase dithering must be applied. The optimal dithering would be a kind of genie dithering such that every sample s_k lies on a decision boundary, since this minimizes the information loss due to 1-bit quantization (see Fig. 1). Heuristics that approximate this genie dithering were investigated in [13]. One can show that if $|s_k|$ is independent of θ, genie phase dithering will result in $\chi(\theta) = \frac{2}{\pi}$, regardless of the SNR or the parameter θ. Thus, the FI is simply given by

$$\mathbf{F}_\mathbf{y} = \frac{2}{\pi}\mathbf{F}_\mathbf{r}, \tag{38}$$

i.e., the same as for low SNR. However, a drawback is that such a receiver requires a feedback from the digital domain to the analog domain, i.e., a voltage-controlled oscillator (VCO) is required that realizes the arbitrary phase rotations that are

required to ensure that every sample s_k lies on a decision boundary. In other words, this results in a digitally controlled PLL. This is due to the fact that the phase dithering for s_k is computed based on the previous samples. Moreover, such a design imposes practical constraints, since one has to make sure that the PLL can lock at a specific phase. If every sample s_k should lie on a decision threshold when the PLL is locked, all samples s_k are required to have the same phase modulo $\frac{\pi}{2}$. This imposes constraints on the modulation alphabet as well as on the receiver design. At first timing synchronization must be performed such that the offset ϵ is removed and the receiver samples the input waveform at the time instants of the transmit symbols. If QPSK modulation is used, all symbols have the same phase modulo $\frac{\pi}{2}$ and feedback based dithering can be applied. All subsequent receiver tasks are then performed at symbol rate.[1] Thus, in [13] perfect timing synchronization and overdemodulation instead of oversampling was considered. An alternative would be to separately dither the amplitudes of $\mathrm{Re}\{s_k\}$ and $\mathrm{Im}\{s_k\}$, like it was proposed for real valued signals in [29]. However, instead of a VCO an AGC is now required, since amplitude dithering requires the amplitude of the signal to lie within the range of the dither signal. An advantage over phase dithering is that genie dithering that is applied separately to $\mathrm{Re}\{s_k\}$ and $\mathrm{Im}\{s_k\}$ can achieve (38) for any $\boldsymbol{\theta}$.

To enable a simple receiver design without any VCO or AGC while removing the phase dependency, we propose the application of a uniformly distributed phase dither φ_k such that $\arg(s_k) \sim \mathcal{U}[0, 2\pi]$. This technique was labeled as inferior to feedback based dithering in [13], but enables a much simpler receiver design since it can be implemented by sampling at a low IF, i.e., $\varphi_k = kT_s\Omega_{\mathrm{IF}}$. If $\frac{T_s\Omega_{\mathrm{IF}}}{\pi}$ is an irrational number, every sample s_k will have a different phase, regardless of all other signal parameters. Thus, for a large number of samples, we can apply the probabilistic model $\arg(s_k) \sim \mathcal{U}[0, 2\pi]$. Due to the law of large numbers, the uniform phase dithering will average out the phase dependency, a fact that has already been observed for the case of phase and frequency estimation of a complex sinusoid in [30]. Such a receiver will inevitably have inferior performance in terms of parameter estimation compared to a receiver that has a feedback from the digital to the analog domain, i.e., approximates the genie dithering. Thus, we aim at analyzing the FI of ϕ, Ω, and ϵ in case of uniform phase dithering, in order to assess the parameter estimation performance of such a receiver.

C. Colored Noise

In order for the noise to be white, we must adapt the receive filter bandwidth to the oversampling factor, i.e., $W_r = \frac{1}{2T_s}$. However, in practice the receive filter bandwidth will be adapted to the bandwidth of the noiseless receive signal to remove all noise outside the signal bandwidth. Oversampling will now result in colored noise, see (4). Unfortunately, it is a mathematically open problem to find an analytical description for the likelihood function $p(\mathbf{y}|\mathbf{s}(\boldsymbol{\theta}))$ in case of colored noise and 1-bit quantization, since there is no analytical description of the orthant probabilities [16, Chapter 2]. Thus, it is impossible to directly derive the FI and the CRLB. However, for real valued signals where an analytical description of the likelihood function is not available or the FI is too difficult to compute, Stein et al. derived a lower bound on the FI that requires only the first and second order moments of $\mathbf{y}$ conditioned on $\mathbf{s}(\boldsymbol{\theta})$ [17]. This bound is a special case of a bounding technique based on the exponential model that was already presented in [31] and generalized and thoroughly studied in [32]. Applications of that bound to 1-bit quantization can be found for real valued signals in [18] and for I-Q receivers in [33] and [34]. However, in [33] and [34] the I and Q components are stacked such that the system model is completely real valued. In order to directly apply this bound to complex valued signals, we applied the FI chain rule [35, Lemma 1] in [19] yielding

$$\mathbf{F}_{\mathbf{y}} = \mathbf{F}_{\mathrm{Re}\{\mathbf{y}\}} + \mathbf{F}_{\mathrm{Im}\{\mathbf{y}\}|\mathrm{Re}\{\mathbf{y}\}} \tag{39}$$

$$\geq \breve{\mathbf{F}}_{\mathrm{Re}\{\mathbf{y}\}} + \breve{\mathbf{F}}_{\mathrm{Im}\{\mathbf{y}\}|\mathrm{Re}\{\mathbf{y}\}}, \tag{40}$$

where $\breve{\mathbf{F}}$ is the FI lower bound derived in [17]. In case $\mathrm{Re}\{\mathbf{y}\}$ and $\mathrm{Im}\{\mathbf{y}\}$ are independent, the bound simplifies to

$$\mathbf{F}_{\mathbf{y}} = \mathbf{F}_{\mathrm{Re}\{\mathbf{y}\}} + \mathbf{F}_{\mathrm{Im}\{\mathbf{y}\}} \tag{41}$$

$$\geq \breve{\mathbf{F}}_{\mathrm{Re}\{\mathbf{y}\}} + \breve{\mathbf{F}}_{\mathrm{Im}\{\mathbf{y}\}} \tag{42}$$

$$= \left(\frac{\partial \boldsymbol{\mu}_{\mathrm{Re}\{\mathbf{y}\}}}{\partial \boldsymbol{\theta}}\right)^T \mathbf{R}^{-1}_{\mathrm{Re}\{\mathbf{y}\}} \left(\frac{\partial \boldsymbol{\mu}_{\mathrm{Re}\{\mathbf{y}\}}}{\partial \boldsymbol{\theta}}\right) + \left(\frac{\partial \boldsymbol{\mu}_{\mathrm{Im}\{\mathbf{y}\}}}{\partial \boldsymbol{\theta}}\right)^T \mathbf{R}^{-1}_{\mathrm{Im}\{\mathbf{y}\}} \left(\frac{\partial \boldsymbol{\mu}_{\mathrm{Im}\{\mathbf{y}\}}}{\partial \boldsymbol{\theta}}\right), \tag{43}$$

where $\boldsymbol{\mu}_{\mathrm{Re}\{\mathbf{y}\}}$ and $\mathbf{R}_{\mathrm{Re}\{\mathbf{y}\}}$ are the first and second order moments

$$\boldsymbol{\mu}_{\mathrm{Re}\{\mathbf{y}\}} = \mathrm{E}\left[\mathrm{Re}\{\mathbf{y}\}|\mathbf{s}(\boldsymbol{\theta})\right] \tag{44}$$

$$\mathbf{R}_{\mathrm{Re}\{\mathbf{y}\}} = \mathrm{E}\left[\mathrm{Re}\{\mathbf{y}\}\,\mathrm{Re}\{\mathbf{y}\}^T|\mathbf{s}(\boldsymbol{\theta})\right], \tag{45}$$

and $\boldsymbol{\mu}_{\mathrm{Im}\{\mathbf{y}\}}$ and $\mathbf{R}_{\mathrm{Im}\{\mathbf{y}\}}$ are defined accordingly.

Following [18], it holds that

$$\left[\boldsymbol{\mu}_{\mathrm{Re}\{\mathbf{y}\}}\right]_k = p(\mathrm{Re}\{y_k\} = +1|\mathbf{s}) - p(\mathrm{Re}\{y_k\} = -1|\mathbf{s}) \tag{46}$$

$$= 1 - 2Q\left(\frac{\mathrm{Re}\{s_k\}}{\sqrt{\left[\mathbf{R}_{\boldsymbol{\eta}}\right]_{kk}/2}}\right), \tag{47}$$

and the derivative is given by

$$\frac{\partial\left[\boldsymbol{\mu}_{\mathrm{Re}\{\mathbf{y}\}}\right]_k}{\partial\theta_i} = \frac{2\exp\left\{-\frac{\mathrm{Re}\{s_k(\boldsymbol{\theta})\}^2}{\left[\mathbf{R}_{\boldsymbol{\eta}}\right]_{kk}}\right\}\frac{\partial}{\partial\theta_i}\mathrm{Re}\{s_k(\boldsymbol{\theta})\}}{\sqrt{\pi\left[\mathbf{R}_{\boldsymbol{\eta}}\right]_{kk}}}. \tag{48}$$

Moreover, the diagonal elements of the covariance matrix are given by

$$\left[\mathbf{R}_{\mathrm{Re}\{\mathbf{y}\}}\right]_{kk} = 1 - \left[\boldsymbol{\mu}_{\mathrm{Re}\{\mathbf{y}\}}\right]_k^2, \tag{49}$$

while the off-diagonal elements are calculated as

$$\left[\mathbf{R}_{\mathrm{Re}\{\mathbf{y}\}}\right]_{kl} = 4p(z_k \leq 0, z_l \leq 0) - \left(1 - \left[\boldsymbol{\mu}_{\mathrm{Re}\{\mathbf{y}\}}\right]_k\right)\left(1 - \left[\boldsymbol{\mu}_{\mathrm{Re}\{\mathbf{y}\}}\right]_l\right) \tag{50}$$

[1] Timing synchronization is usually the first block in standard receivers, since timing synchronized samples at symbol rate give a sufficient statistic for phase estimation and symbol detection [24]. However, this argument is invalid in case of 1-bit quantization.

where $[z_k, z_l]^T$ is a bi-variate Gaussian random vector

$$\begin{bmatrix} z_k \\ z_l \end{bmatrix} \sim \mathcal{N}\left(\begin{bmatrix} \mathrm{Re}\left\{s_k(\boldsymbol{\theta})\right\} \\ \mathrm{Re}\left\{s_l(\boldsymbol{\theta})\right\} \end{bmatrix}, \frac{1}{2} \begin{bmatrix} \left[\mathbf{R}_{\boldsymbol{\eta}}\right]_{kk} & \left[\mathbf{R}_{\boldsymbol{\eta}}\right]_{kl} \\ \left[\mathbf{R}_{\boldsymbol{\eta}}\right]_{lk} & \left[\mathbf{R}_{\boldsymbol{\eta}}\right]_{ll} \end{bmatrix} \right). \tag{51}$$

Thus, (50) can only be obtained numerically. The lower bound for the FI of $\mathrm{Im}\{\mathbf{y}\}$ is derived in the same manner. Unfortunately, the quality of the bound, i.e., its tightness, is to the best of our knowledge unknown in the general case. However, in case the noise is white where the FI can be computed, it was shown in [17] for the simple signal model $\mathrm{sign}_\alpha(\theta+\eta)$, where $\eta \sim \mathcal{N}(0,\sigma^2)$ and $\mathrm{sign}_\alpha(\cdot)$ is the 1-bit quantizer with threshold α, that the FI lower bound equals the actual FI, i.e. the bound is tight. This result carries over to the general, multivariate and complex valued signal model $\mathrm{csign}\left(\mathbf{s}(\boldsymbol{\theta})+\boldsymbol{\eta}\right)$ [19].

V. Fisher Information with White Noise and Uniform Phase Dithering

In the following we study the FI in case uniform phase dithering and 1-bit quantization is applied at the receiver. To gain a deeper insight, we will stick to the white noise assumption, i.e., $W_r = \frac{1}{2T_s}$, which enables an analytical treatment. We first present a closed form for the FI of a general signal model averaged over the phase. Subsequently in Section V-B we apply this result to the estimation of $\boldsymbol{\theta} = [\phi, \epsilon, \Omega]$ from the receive signal defined in Section II. We will argue that the estimation of the timing parameter ϵ requires the oversampling factor $M = \frac{T}{T_s}$ to be an irrational number in order to average out the non-linear behavior due to 1-bit quantization. Moreover, considering known i.i.d. transmit symbols, in Section V-C we obtain very tight closed form lower bounds on the CRLB of $\boldsymbol{\theta} = [\phi, \epsilon, \Omega]$.

A. General signal model

In order to enable an analytical treatment in the following derivations, we will apply a very close approximation to (30) that we proposed in [21]. Since the function $B(x)$ (see (30)) is very close to a Gaussian function we will use the approximation

$$B(x) = \frac{e^{-x^2}}{Q(x)Q(-x)} \approx c_1 e^{-c_2 x^2}, \tag{52}$$

where c_1 and c_2 are constants that are obtained by numerically solving

$$[c_1, c_2] = \arg\min_{c_1,c_2} \int_0^R \left| \frac{e^{-x^2}}{Q(x)Q(-x)} - c_1 e^{-c_2 x^2} \right| dx. \tag{53}$$

For $R = 10$ we obtain the values $c_1 = 4.0360$ and $c_2 = 0.3930$, which do not change for the considered numerical accuracy if we choose R even higher. The absolute approximation error, shown in Fig. 3, is very small for all values of x, with a maximum of 0.036 at $x = 0$. On the other hand, for large x we observe that the error is larger than the approximated function. However, this does not pose a problem in our case, since the relative error is only large where the value of $B(x)$ is very small. i.e., the contribution to the FI is very small when

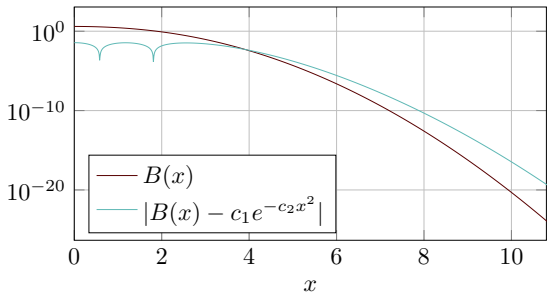

Fig. 3: Absolute approximation error of $B(x)$

the relative error is large. With (52) we can now approximate (30) with

$$\left[\tilde{\mathbf{F}}_{\mathbf{y}}\right]_{\theta_i\theta_j} = \frac{c_1}{\pi\sigma^2} \sum_k \left(e^{-c_2 \frac{(\mathrm{Re}\{s_k\})^2}{\sigma^2/2}} \frac{\partial}{\partial\theta_i}\mathrm{Re}\left\{s_k\right\} \frac{\partial}{\partial\theta_j}\mathrm{Re}\left\{s_k\right\} + e^{-c_2 \frac{(\mathrm{Im}\{s_k\})^2}{\sigma^2/2}} \frac{\partial}{\partial\theta_i}\mathrm{Im}\left\{s_k\right\} \frac{\partial}{\partial\theta_j}\mathrm{Im}\left\{s_k\right\} \right), \tag{54}$$

where $\tilde{\mathbf{F}}_{\mathbf{y}}$ denotes the FI computed using the approximation (52). Before stating the central theorem of this section, we have to introduce the following lemma.

Lemma 1: For $x \in \mathbb{C}$

$$\int_0^{2\pi} e^{-x\cos^2(\gamma)} \sin^2(\gamma)\, d\gamma = \int_0^{2\pi} e^{-x\sin^2(\gamma)} \cos^2(\gamma)\, d\gamma \tag{55}$$

$$= \pi e^{-\frac{x}{2}} \left(I_0\left(\frac{x}{2}\right) + I_1\left(\frac{x}{2}\right) \right) \tag{56}$$

and

$$\int_0^{2\pi} e^{-x\cos^2(\gamma)} \cos^2(\gamma)\, d\gamma = \int_0^{2\pi} e^{-x\sin^2(\gamma)} \sin^2(\gamma)\, d\gamma \tag{57}$$

$$= \pi e^{-\frac{x}{2}} \left(I_0\left(\frac{x}{2}\right) - I_1\left(\frac{x}{2}\right) \right), \tag{58}$$

where $I_v(\cdot)$ are the modified Bessel functions of the first kind. Moreover,

$$\int_0^{2\pi} e^{-x\cos^2(\gamma)} \cos(\gamma)\sin(\gamma)\, d\gamma = \int_0^{2\pi} e^{-x\sin^2(\gamma)} \cos(\gamma)\sin(\gamma)\, d\gamma \tag{59}$$

$$= 0. \tag{60}$$

Proof: A proof of (56) is given in [21] and the proof of (58) and (60) is analogous. ∎

We can now state the following theorem.

Theorem 1: Let

$$\mathbf{y} = \mathrm{csign}\left(\mathbf{s}(\boldsymbol{\theta}) + \boldsymbol{\eta}\right) \tag{61}$$

where $\mathbf{s}(\boldsymbol{\theta}) \in \mathbb{C}^K$, $\boldsymbol{\theta} \in \mathbb{R}^L$, and $\boldsymbol{\eta} \sim \mathcal{CN}\left(\mathbf{0}, \mathbf{R}_{\boldsymbol{\eta}}\right)$ is a circularly-symmetric complex Gaussian random vector with independent

real and imaginary part. Furthermore, $\mathbf{s}(\boldsymbol{\theta})$ and $\boldsymbol{\eta}$ are independent, and we assume uniform phase dithering such that $\arg(s_k(\boldsymbol{\theta})) = \gamma_k(\boldsymbol{\theta}) \sim \mathcal{U}(0, 2\pi)$. For $K \to \infty$

$$\left[\tilde{\mathbf{F}}_{\mathbf{y}}\right]_{\theta_i\theta_j} = \frac{1}{\pi\sigma^2}\sum_k \left(\kappa_0\left(\frac{|s_k|^2}{\sigma^2}\right)\frac{\partial|s_k|}{\partial\theta_i}\frac{\partial|s_k|}{\partial\theta_j} + \kappa_1\left(\frac{|s_k|^2}{\sigma^2}\right)\frac{\partial\gamma_k}{\partial\theta_i}\frac{\partial\gamma_k}{\partial\theta_j}|s_k|^2\right), \quad (62)$$

where, as before, we dropped $\boldsymbol{\theta}$ from s_k for notational convenience. The functions $\kappa_0(x)$ and $\kappa_1(x)$ are defined as

$$\kappa_0(x) = c_1 e^{-c_2 x}\left(I_0(c_2 x) - I_1(c_2 x)\right) \quad (63)$$

and

$$\kappa_1(x) = c_1 e^{-c_2 x}\left(I_0(c_2 x) + I_1(c_2 x)\right). \quad (64)$$

Proof: With $\mathrm{Re}\{s_k\} = |s_k|\cos(s_k)$, $\mathrm{Im}\{s_k\} = |s_k|\sin(s_k)$, and the elementary rules of differentiation, we reformulate (54) and obtain (65), which can be seen at the top of the page. Due to the law of large numbers, $\frac{1}{K}\left[\tilde{\mathbf{F}}_{\mathbf{y}}\right]_{\theta_i\theta_j} \xrightarrow{p} \mathrm{E}\left[\left[\tilde{\mathbf{F}}_{y_k}\right]_{\theta_i\theta_j}\right]$, where $\xrightarrow{p}$ means convergence in probability. Thus, for $K \to \infty$ the FI equals its average over γ_k such that (62) follows directly from $\gamma_k \sim \mathcal{U}(0, 2\pi)$, Lemma 1, the linearity of the expectation operation and the fact that $\frac{\partial\gamma_k}{\partial\theta_i}$ is a constant w.r.t. the expectation over γ_k as the dithering is independent of $\boldsymbol{\theta}$. ∎

Since the direct computation of the derivatives of $|s_k|$ and γ_k might be difficult, we provide different representations of (62) in the following corollary, where the proof is given in Appendix B.

Corollary 1: Let us consider the assumptions made in Theorem 1. For $K \to \infty$, (62) can equivalently be expressed as

$$\left[\tilde{\mathbf{F}}_{\mathbf{y}}\right]_{\theta_i\theta_j} = \frac{1}{\pi\sigma^2}\sum_k \left(\kappa_0\left(\frac{|s_k|^2}{\sigma^2}\right)\frac{\mathrm{Re}\left\{s_k^*\frac{\partial}{\partial\theta_i}s_k\right\}\mathrm{Re}\left\{s_k^*\frac{\partial}{\partial\theta_j}s_k\right\}}{|s_k|^2} + \kappa_1\left(\frac{|s_k|^2}{\sigma^2}\right)\frac{\mathrm{Im}\left\{s_k^*\frac{\partial}{\partial\theta_i}s_k\right\}\mathrm{Im}\left\{s_k^*\frac{\partial}{\partial\theta_j}s_k\right\}}{|s_k|^2}\right). \quad (66)$$

Moreover, if $i = j$,

$$\left[\tilde{\mathbf{F}}_{\mathbf{y}}\right]_{\theta_i\theta_i} = \frac{1}{\pi\sigma^2}\sum_k \left(\kappa_1\left(\frac{|s_k|^2}{\sigma^2}\right)\frac{\partial}{\partial\theta_i}s_k^*\frac{\partial}{\partial\theta_i}s_k - \kappa_2\left(\frac{|s_k|^2}{\sigma^2}\right)\left(\frac{\partial}{\partial\theta_i}|s_k|\right)^2\right), \quad (67)$$

where

$$\kappa_2(x) = \kappa_1(x) - \kappa_0(x) \quad (68)$$

$$= 2c_1 e^{-c_2 x} I_1(c_2 x). \quad (69)$$

B. Phase, timing, and frequency estimation

Applying Theorem 1 to the joint estimation of $\boldsymbol{\theta} = [\phi, \epsilon, \Omega]$ leads to the following theorem, where the proof is given in Appendix C.

Theorem 2: Let us consider the 1-bit quantized receive signal

$$y_k = \mathrm{csign}(s_k(\boldsymbol{\theta}) + \eta_k), \quad (70)$$

as defined in Section II. Moreover, we assume that $W_r = 1/(2T_s)$ such that $\mathbf{R}_{\boldsymbol{\eta}} = (N_0/T_s)\mathbf{I} = \sigma^2\mathbf{I}$. If we assume that the N transmit symbols $\{a_n\}$ are i.i.d. and known, that the signal pulse $g(t)$ is real valued, and that uniform phase dithering $\varphi_k \sim \mathcal{U}(0, 2\pi)$ is applied, for $N \to \infty$ the FI matrix of $\boldsymbol{\theta} = [\phi, \epsilon, \Omega]$ is given by,

$$\left[\tilde{\mathbf{F}}_{\mathbf{y}}\right]_{\phi\phi} = \frac{1}{\pi(N_0/T_s)}\sum_k \kappa_1\left(\frac{|s_k|^2}{N_0/T_s}\right)|s_k|^2 \quad (71)$$

$$\left[\tilde{\mathbf{F}}_{\mathbf{y}}\right]_{\Omega\Omega} = \frac{1}{\pi(N_0/T_s)}\sum_k \kappa_1\left(\frac{|s_k|^2}{N_0/T_s}\right)k^2T_s^2|s_k|^2 \quad (72)$$

$$\left[\tilde{\mathbf{F}}_{\mathbf{y}}\right]_{\epsilon\epsilon} = \frac{1}{\pi(N_0/T_s)}\sum_k \left(\kappa_1\left(\frac{|s_k|^2}{N_0/T_s}\right)\frac{\partial}{\partial\epsilon}s_k^*\frac{\partial}{\partial\epsilon}s_k - \kappa_2\left(\frac{|s_k|^2}{N_0/T_s}\right)\left(\frac{\partial}{\partial\epsilon}|s_k|\right)^2\right) \quad (73)$$

$$\left[\tilde{\mathbf{F}}_{\mathbf{y}}\right]_{\phi\Omega} = \frac{1}{\pi(N_0/T_s)}\sum_k \kappa_1\left(\frac{|s_k|^2}{N_0/T_s}\right)kT_s|s_k|^2 \quad (74)$$

$$\left[\tilde{\mathbf{F}}_{\mathbf{y}}\right]_{\epsilon\phi} = 0 \quad (75)$$

$$\left[\tilde{\mathbf{F}}_{\mathbf{y}}\right]_{\epsilon\Omega} = 0. \quad (76)$$

$$\left[\tilde{\mathbf{F}}_{\mathbf{y}}\right]_{\theta_i\theta_j} = \frac{c_1}{\pi\sigma^2}\sum_k \left[e^{\frac{-c_2|s_k|^2\cos^2(\gamma_k)}{\sigma^2/2}}\left(\frac{\partial|s_k|}{\partial\theta_i}\frac{\partial|s_k|}{\partial\theta_j}\cos^2(\gamma_k) + \frac{\partial\gamma_k}{\partial\theta_i}\frac{\partial\gamma_k}{\partial\theta_j}|s_k|^2\sin^2(\gamma_k) - \left(\frac{\partial|s_k|}{\partial\theta_i}\frac{\partial\gamma_k}{\partial\theta_j} + \frac{\partial\gamma_k}{\partial\theta_i}\frac{\partial|s_k|}{\partial\theta_j}\right)|s_k|\cos(\gamma_k)\sin(\gamma_k)\right) + e^{\frac{-c_2|s_k|^2\sin^2(\gamma_k)}{\sigma^2/2}}\left(\frac{\partial|s_k|}{\partial\theta_i}\frac{\partial|s_k|}{\partial\theta_j}\sin^2(\gamma_k) + \frac{\partial\gamma_k}{\partial\theta_i}\frac{\partial\gamma_k}{\partial\theta_j}|s_k|^2\cos^2(\gamma_k) + \left(\frac{\partial|s_k|}{\partial\theta_i}\frac{\partial\gamma_k}{\partial\theta_j} + \frac{\partial\gamma_k}{\partial\theta_i}\frac{\partial|s_k|}{\partial\theta_j}\right)|s_k|\cos(\gamma_k)\sin(\gamma_k)\right)\right] \quad (65)$$

At first we observe that due to uniform phase dithering, the efficient estimator $\hat{\epsilon}$ is orthogonal to $\hat{\Omega}$ and $\hat{\phi}$ if we assume random data and real valued pulses $g(t)$, i.e., this property of the unqantized receiver is preserved. Looking at Fig. 2, it is intuitively clear that uniform phase dithering will average out the correlation that $\hat{\epsilon}$ has with $\hat{\phi}$ and $\hat{\Omega}$. Moreover, we observe that due to uniform phase dithering the values of ϕ and Ω have no influence on any of the elements of the FI matrix. The growth rate of $\left[\tilde{\mathbf{F}}_{\mathbf{y}}\right]_{\theta_i\theta_j}$ w.r.t. N is given in the following corollary.

Corollary 2: Let us consider the assumptions from Theorem 2. If $\left[\tilde{\mathbf{F}}_{\mathbf{r}}\right]_{\theta_i\theta_j}$ grows with $O\left(f\left(N\right)\right)$, then $\left[\tilde{\mathbf{F}}_{\mathbf{y}}\right]_{\theta_i\theta_j}$ also grows with $O\left(f\left(N\right)\right)$, where $\boldsymbol{\theta} = [\phi, \epsilon, \Omega]$.

Proof: Observing (71), (72), and (74), we recognize that the FI is identical to the unquantized case, except that the contribution of each sample is scaled by the monotone decreasing function $\kappa_1(\cdot)$ that depends on the SNR in the particular sample. Since $\frac{|s_k|^2}{N_0/T_s}$ is independent of N, this scaling does not influence the growth rate with N. The same discussion holds for (73), except for an additional subtractive term. However, since (73) must be positive and cannot grow faster than with $O\left(f\left(N\right)\right)$ due to (34), it must also grow with $O\left(f\left(N\right)\right)$. ■

This corollary states the important result that an efficient estimator has no loss in the growth rate with N, in comparison to the unquantized receiver, if 1-bit quantization with uniform phase dithering is applied. Moreover, from Theorem 2, Corollary 2, and (28), we can immediately infer that for $N \to \infty$

$$\left[\tilde{\mathbf{F}}_{\mathbf{y}}^{-1}\right]_{\theta_i\theta_i} = \left[\tilde{\mathbf{F}}_{\mathbf{y}}\right]^{-1}_{\theta_i\theta_i}, \tag{77}$$

i.e., the influence of the cross terms in the FI matrix is negligible for large N.

Since for $N \to \infty$ and i.i.d. data $[\mathbf{F}_{\mathbf{r}}]_{\theta_i\theta_j} \xrightarrow{p} \mathrm{E}_{\{a_n\}}\left[[\mathbf{F}_{\mathbf{r}}]_{\theta_i\theta_j}\right]$, closed form solutions could be given for the unquantized receiver [26, Chapter 6.2], as recalled in Section III. From these closed forms it was easy to see how different system parameters, e.g., the pulse form $g(t)$, influence the FI matrix. Unfortunately, no such closed forms are available for the receiver with 1-bit quantization. To this end, we will derive very tight closed form upper bounds on the FI, i.e., lower bounds on the CRLB, in Section V-C.

However, beforehand we want to argue that uniform phase dithering does not sufficiently reduce the effect of the non-linearity introduced by 1-bit quantization when estimating the timing parameter ϵ. The CRLB of ϵ is plotted in Fig. 4. At first we observe that at low $\frac{E_s}{N_0}$, the performance is better if the roll-off factor of $g(t)$ is high, a property that we already know from the unquantized receiver. However, at medium to high $\frac{E_s}{N_0}$, the performance is increasingly sensitive on the value of ϵ, while in the unquantized case the performance is independent of ϵ. Furthermore, how sensitive the receiver will be on a change in ϵ depends on the roll-off factor of the pulse form $g(t)$. The higher the roll-off factor, the more sensitive is the CRLB on the actual value of ϵ. In case of ϕ and Ω we observed, not plotted here, that the CRLB is independent from the timing parameter ϵ. This observation has a simple explanation. Changing ϵ has

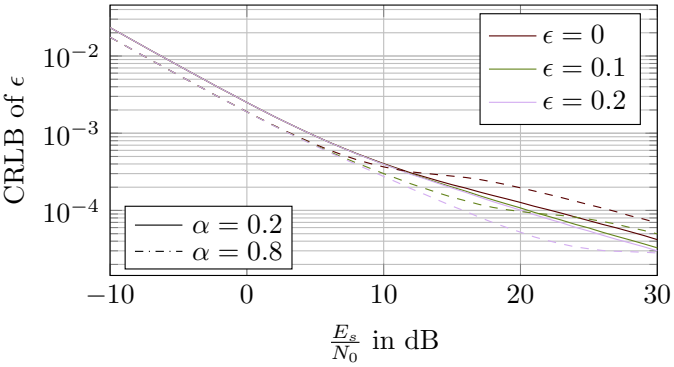

Fig. 4: CRLB of ϵ for $N = 100$, $M = 3$, $T = 1$, and root raised cosine pulses $g(t)$, obtained by Monte Carlo simulations over 1000 random sequences $\{a_n\}$.

an influence on the distribution of $|s_k|$ and $\arg(s_k)$. In case of uniform phase dithering $\arg(s_k) \sim \mathcal{U}(0, 2\pi)$, and thus ϵ has no influence on the distribution of $\arg(s_k)$ anymore. Hence, for large N the value ϵ has no larger influence on the CRLB of ϕ and Ω than it has in the unquantized case, since ϕ and Ω do not affect $|s_k|$. However, ϵ still has influence on the distribution of $|s_k|$, since $|s_k|$ is not dithered. Thus, the CRLB of ϵ is highly sensitive on the actual value of ϵ.

To overcome this, one could dither $|s_k|$. However, this seems rather impracticable and would require an AGC at the receiver. A better alternative is to dither the sampling time such that $\left[\tilde{\mathbf{F}}_{\mathbf{y}}\right]_{\epsilon\epsilon} \xrightarrow{p} \mathrm{E}_{\epsilon}\left[\left[\tilde{\mathbf{F}}_{\mathbf{y}}\right]_{\epsilon\epsilon}\right]$ for $N \to \infty$, where $\epsilon \sim \mathcal{U}(-0.5, 0.5)$. This can easily be achieved without actually making ϵ random. One only has to ensure that $M = \frac{T}{T_s}$ is an irrational number. In order to explain this, let us introduce the concept of the sampling phase, i.e., the time difference of a sample s_k to its respective transmit symbol. In Fig. 4 we chose $M = 3$, i.e., M is an integer. This causes the effect that the pattern of relative time differences between the transmit symbol and its corresponding samples s_k is the same for each transmit symbol, i.e., the sample phase is periodic in M. However, if M is an irrational number every sample has a different sampling phase, even if $N \to \infty$. Thus, $\left[\tilde{\mathbf{F}}_{\mathbf{y}}\right]_{\epsilon\epsilon} \xrightarrow{p} \mathrm{E}_{\epsilon}\left[\left[\tilde{\mathbf{F}}_{\mathbf{y}}\right]_{\epsilon\epsilon}\right]$ for $N \to \infty$, without actually dithering the sampling. The effect is the same that sampling at a normalized irrational intermediate frequency has on the phase (see Section IV). When $\frac{T_s\Omega_{IF}}{\pi}$ is irrational, every sample s_k has a different phase and when M is irrational, every sample has a different sampling phase. This averages out the effect of the non-linearity of the 1-bit quantization.

It may seem that M being irrational is a rather theoretical assumption. However, the opposite is the case. Since the clocks at transmitter and receiver are not synchronized in general M will be an irrational number [26, Section 4.1.1].

C. Lower bounds on the CRLB

Here we want to give very tight closed form lower bounds on the CRLB of $\boldsymbol{\theta} = [\phi, \epsilon, \Omega]$. If we additionally to the setting

of Theorem 2 assume that $M = \frac{T_s}{T}$ is an irrational number, for $N \to \infty$ the CRLB of $\boldsymbol{\theta} = [\phi, \epsilon, \Omega]$ is lower-bounded by

$$\left[\tilde{\mathbf{F}}_{\mathbf{y}}^{-1}\right]_{\theta_i\theta_i} = \left[\tilde{\mathbf{F}}_{\mathbf{y}}\right]^{-1}_{\theta_i\theta_i} \tag{78}$$

$$\geq \left(\frac{1}{2\pi}\kappa_1\left(\frac{E_s}{N_0 M}\right)\right)^{-1} [\mathbf{F}_{\mathbf{r}}]^{-1}_{\theta_i\theta_i}. \tag{79}$$

For ϕ and Ω the bound (79) is proven in Appendix D. However, the bounding of the FI of ϵ is based on numerical evaluation as we have not been able to rigorously prove (79) for ϵ. These numerical evaluations show that for raised cosine and root raised cosine pulses $g(t)$ the provided lower bound on the CRLB holds.

We observe that the bound (79) equals the CRLB of the unquantized receiver multiplied by a loss factor that depends only on $\frac{E_s}{N_0}$ and the oversampling factor M, where $\frac{E_s}{N_0 M}$ is in fact the SNR. Thus, we can use the closed form solutions given for $\mathbf{F}_{\mathbf{r}}$ in Section III to obtain (79). In order to gain a deeper understanding of the impact of the loss factor, we approximate the bound in (79) for low and high SNR with

$$\left[\tilde{\mathbf{F}}_{\mathbf{y}}^{-1}\right]_{\theta_i\theta_i} = \left[\tilde{\mathbf{F}}_{\mathbf{y}}\right]^{-1}_{\theta_i\theta_i} \tag{80}$$

$$\geq \begin{cases} \frac{\pi}{2}[\mathbf{F}_{\mathbf{r}}]^{-1}_{\theta_i\theta_i} & \text{for low SNR} \\ \frac{\sqrt{2\pi^3 c_2}}{c_1}\sqrt{\frac{E_s}{N_0}}\frac{1}{\sqrt{M}}[\mathbf{F}_{\mathbf{r}}]^{-1}_{\theta_i\theta_i} & \text{for high SNR,} \end{cases} \tag{81}$$

where the low SNR result follows directly from (34) and the high SNR result follows from the approximation [36, Eq. (10.30.4)]

$$I_\nu(x) \approx \frac{e^x}{\sqrt{2\pi x}} \tag{82}$$

for $x \to \infty$ such that

$$\kappa_1(x) \approx \frac{2c_1}{\sqrt{2\pi c_2 x}}. \tag{83}$$

As can be seen, there are two major differences between the low and the high SNR regime. In the low SNR, the behavior is identical to the unquantized case, i.e., the performance improves with $O\left(\frac{E_s}{N_0}\right)$ and oversampling has no effect. On the other hand, as $[\mathbf{F}_{\mathbf{r}}]^{-1}_{\theta_i\theta_i}$ improves with $O\left(\frac{E_s}{N_0}\right)$ (see (24) – (27)), $\left[\mathbf{F}_{\mathbf{y}}\right]^{-1}_{\theta_i\theta_i}$ improves with $O\left(\sqrt{\frac{E_s}{N_0}}\right)$ in the high SNR regime, due to the factor $\sqrt{\frac{E_s}{N_0}}$ in (81). In case of the simpler problem of phase and frequency estimation of a complex sinusoid, it has already been observed in [30] that the performance improves only with the square root of the SNR in the high SNR regime, if the phase dependency has been averaged out due to an irrational frequency of the sinusoid. Moreover, as increasing M decreases the SNR, oversampling is shifting the regime up to which the low SNR approximation holds to a higher $\frac{E_s}{N_0}$, i.e., for $M \to \infty$ the performance loss compared to the unquantized receiver will converge to the low SNR loss of $\frac{2}{\pi}$.

VI. Numerical Evaluation

In this section we want to present a numerical evaluation of our results. At first, we evaluate the results obtained for white noise in Section V. Subsequently, we will compare the CRLB for white noise with the CRLB upper bound for colored noise, given in Section IV-C.

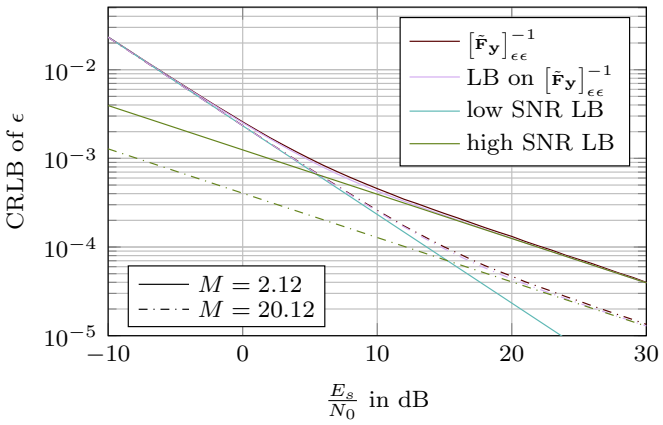

Fig. 5: CRLB of ϵ and its lower bounds (LB) for $N = 100$, $T = 1$, and root raised cosine pulses $g(t)$ with $\alpha = 0.2$, where $\left[\tilde{\mathbf{F}}_{\mathbf{y}}\right]^{-1}_{\epsilon\epsilon}$ was averaged over 1000 random sequences $\{a_n\}$.

A. White Noise

In the following we want to evaluate the bounds derived in Section V for white noise and uniform phase and sample dithering.[2] To this end, Fig. 5 exemplarily depicts $\left[\tilde{\mathbf{F}}_{\mathbf{y}}\right]^{-1}_{\epsilon\epsilon}$ and its bounds. The behavior for ϕ and Ω is analogous. At first we observe that the bound (79) is very tight. Moreover, as predicted by the bounds (81), the CRLB is separated into a low and a high SNR regime, where the performance first improves linearly and than with the square root of $\frac{E_s}{N_0}$. We observe that oversampling is moving the high SNR bound of the CRLB downwards, which also moves the crossing point with the low SNR bound to a higher $\frac{E_s}{N_0}$ point. This is due to the fact that oversampling is decreasing the SNR, since the receive filter must be wider if the noise is required to be white. I.e., as already discussed in Section V-C, oversampling is shifting the regime where the low SNR approximation holds to a higher $\frac{E_s}{N_0}$ and the performance loss compared to the unquantized receiver will converge towards the low SNR loss of $\frac{2}{\pi}$ as $M \to \infty$. Note that the low SNR bound gives the performance that is achievable with the genie dithering, as discussed in Section IV-B.

B. Colored Noise

Finally we want to analyze the influence of noise correlation by assuming that the receive filter is not adapted to the sampling rate, i.e., $W_r = W_g + \frac{|\Omega_{\max}+\Omega_{\mathrm{IF}}|}{2\pi}$, where $\Omega_{\max}$ is the maximum frequency uncertainty. Since the FI cannot be computed directly in this case, we resort to the FI lower bound discussed in Section IV-C, which gives an upper bound on the CRLB. At first, numerical evaluations not presented here show that as proved for white noise in (77), the cross terms in the FI matrix can also be neglected for large N in case of colored noise.

[2]Theoretically M must be an irrational number. However, numerical evaluations show that in practice it is sufficient that M is a rational number with a few decimal places. The same discussion hold for Ω_{IF}.

In Fig. 6, we compare white and colored noise for different oversampling factors. As the CRLB is independent of the frequency uncertainty if uniform phase dithering is applied, we assumed $\Omega_{\max} = 0$ for simplicity. The only difference is that a larger frequency uncertainty will increase the amount of noise captured due to a larger bandwidth of the receive filter, which will reduce the performance gain due to correlation. We observe that also in case of colored noise the CRLB has a smaller slope in the high SNR regime. However, the performance loss compared to the unquantized receiver is reduced, i.e., allowing for noise correlation yields better performance than adapting the receive filter bandwidth to the oversampling factor which results in white noise at the cost of higher noise power. In particular, colored noise can increase the performance beyond the low SNR bound for white noise (34). This observation has already been made in, e.g., [37] and [18], for direction-of-arrival parameter estimation and time-of-arrival estimation, respectively. Furthermore, we observe that colored noise is a little more beneficial for timing estimation than for frequency and phase estimation. The CRLB upper bound for colored noise and $M = 6$ crosses the low SNR bound for white noise at approximately $\frac{E_s}{N_0} \approx 5$ dB in case of phase and frequency estimation and at $\frac{E_s}{N_0} \approx 12$ dB in case of timing estimation.

VII. Conclusion

In this paper we studied the FI and the CRLB of phase, frequency, and timing estimation. We observed that the parameter estimation performance is highly dependent on the phase shift of the input signal. To overcome this problem, we proposed uniformly distributed phase dithering before 1-bit quantization, which can be implemented in practice by low IF sampling. Based on the assumption of white noise due to the adaptation of the receive filter bandwidth to the sampling rate we derived the FI for a general signal under phase dithering and applied the results to phase, frequency, and timing estimation.

Furthermore, we observed that the performance of the estimation of the timing shift is highly dependent on the actual value of the timing shift. Thus, we proposed uniform dithering in the sampling, which can be implemented by assuring that the oversampling factor is an irrational number. Based on Jensen's inequality we derived a very tight lower bound on the CRLB of phase, timing, and frequency, considering dithering in phase and sampling time. This bound shows that the properties that hold for large N for the unquantized receiver, also hold for the 1-bit quantized receiver, if phase and sample dithering are applied, e.g., the phase estimation performance is independent of the pulse form. The only difference is a performance loss that depends on $\frac{E_s}{N_0}$ and the oversampling factor, where increasing the oversampling factor can reduce the performance loss up to the low SNR limit of $\frac{2}{\pi}$. This is also the limit that can be achieved in case of genie aided dithering, e.g., by using feedback from the digital to the analog domain. Moreover, a comparison with the numerically computed CRLB upper bound for colored noise, i.e., the receive filter bandwidth is not adapted to the sampling rate, shows that noise correlation can reduce the performance loss compared to the unquantized receiver.

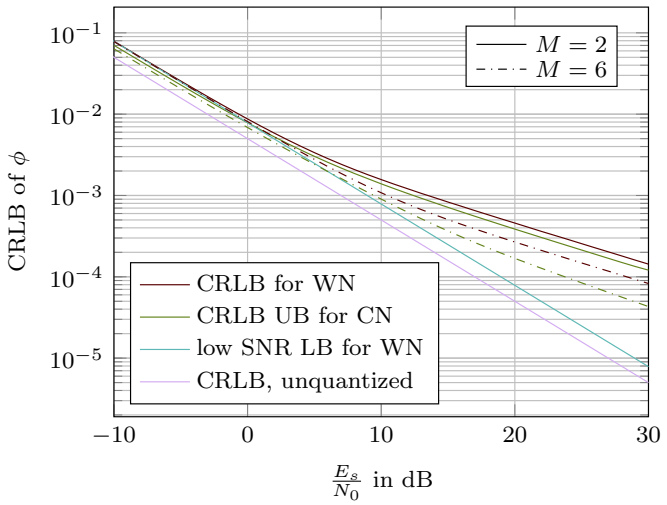

(a) CRLB of ϕ

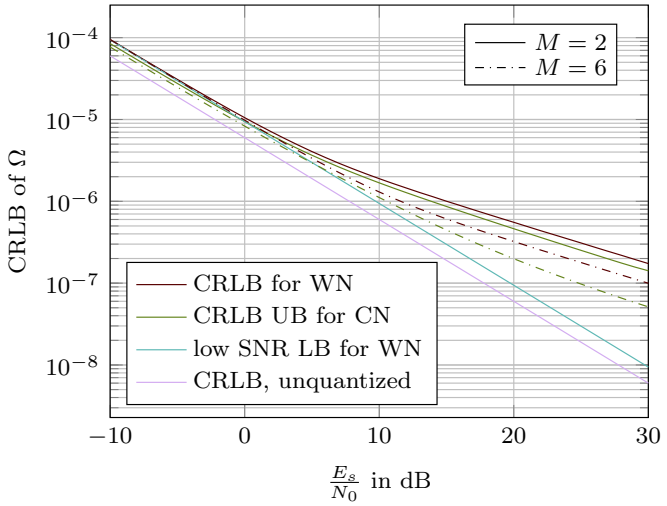

(b) CRLB of Ω

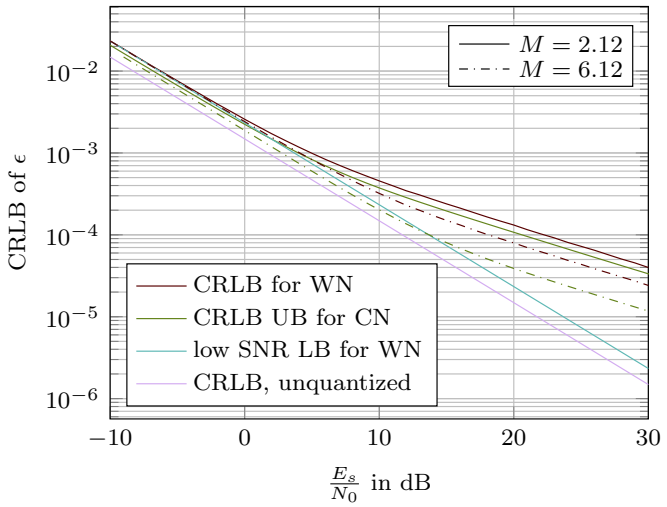

(c) CRLB of ϵ

Fig. 6: CRLB for white noise (WN) compared to the CRLB upper bound (UB) for colored noise (CN) with $N = 100$, $T = 1$, and root raised cosine pulses $g(t)$ with $\alpha = 0.2$, averaged over 1000 random sequences $\{a_n\}$. The CRLB upper bound was computed with $\Omega_{\text{IF}} = 0.12\pi$.

Practically important is the fact that the receiver design required to achieve the aforementioned properties is very simple, neither an AGC, nor any feedback from the digital to the analog domain are required.

Appendix A
Proof of (34)

Proof: As can be seen in (30), due to white noise with independent real and imaginary part, the FI matrix can be written as the sum of the contribution of each sample, i.e.,

$$\mathbf{F}_{\mathbf{y}} = \sum_k \mathbf{F}_{\mathrm{Re}\{y_k\}} + \sum_k \mathbf{F}_{\mathrm{Im}\{y_k\}}. \tag{84}$$

The same is obviously true for $\mathbf{F}_{\mathbf{r}}$. Thus, we only have to prove (34) for one individual contribution $\mathbf{F}_{\mathrm{Re}\{y_k\}}$ to the FI, as it will then also be true for the sum of all contributions, see, e.g., [27, Problem 7.1]. In order to proof (34), we will make use of [27, Theorem 7.7.3], which states that for two positive definite matrices A and C, $A \preceq C$ if and only if $\rho\left(AC^{-1}\right) \leq 1$, where $\rho(\cdot)$ denotes the spectral radius. With (30)

$$\rho\left(\mathbf{F}_{\mathrm{Re}\{y_k\}}\frac{\pi}{2}\mathbf{F}^{-1}_{\mathrm{Re}\{r_k\}}\right) = \rho\left(\frac{1}{2\pi}B\left(\frac{\mathrm{Re}\{s_k\}}{\sigma/\sqrt{2}}\right)\mathbf{F}_{\mathrm{Re}\{r_k\}}\frac{\pi}{2}\mathbf{F}^{-1}_{\mathrm{Re}\{r_k\}}\right) \tag{85}$$

$$= \rho\left(\frac{1}{4}B\left(\frac{\mathrm{Re}\{s_k\}}{\sigma/\sqrt{2}}\right)\mathbf{I}\right) \tag{86}$$

$$= \frac{1}{4}B\left(\frac{\mathrm{Re}\{s_k\}}{\sigma/\sqrt{2}}\right) \tag{87}$$

$$\leq 1, \tag{88}$$

where equality holds for $\sigma \to \infty$. This is true since $B(x)$ is a symmetric and unimodal function with maximum $B(0) = 4$, see Fig. 3. ∎

Appendix B
Proof of Corollary 1

Proof: With

$$\frac{\partial}{\partial\theta_i}|s_k| = \frac{\partial}{\partial\theta_i}\sqrt{\mathrm{Re}\{s_k\}^2 + \mathrm{Im}\{s_k\}^2} \tag{89}$$

$$= \frac{\mathrm{Re}\{s_k\}\frac{\partial}{\partial\theta_i}\mathrm{Re}\{s_k\} + \mathrm{Im}\{s_k\}\frac{\partial}{\partial\theta_i}\mathrm{Im}\{s_k\}}{|s_k|} \tag{90}$$

$$= \frac{\mathrm{Re}\left\{s_k^*\frac{\partial}{\partial\theta_i}s_k\right\}}{|s_k|} \tag{91}$$

and

$$\frac{\partial}{\partial\theta_i}\gamma_k = \frac{\partial}{\partial\theta_i}\arctan\left(\frac{\mathrm{Im}\{s_k\}}{\mathrm{Re}\{s_k\}}\right) \tag{92}$$

$$= \frac{\mathrm{Re}\{s_k\}\frac{\partial}{\partial\theta_i}\mathrm{Im}\{s_k\} - \mathrm{Im}\{s_k\}\frac{\partial}{\partial\theta_i}\mathrm{Re}\{s_k\}}{|s_k|^2} \tag{93}$$

$$= \frac{\mathrm{Im}\left\{s_k^*\frac{\partial}{\partial\theta_i}s_k\right\}}{|s_k|^2} \tag{94}$$

(66) follows directly from (62). Moreover, with

$$\frac{\partial}{\partial\theta_i}s_k^*\frac{\partial}{\partial\theta_i}s_k - \left(\frac{\partial}{\partial\theta_i}|s_k|\right)^2$$

$$= \frac{\partial}{\partial\theta_i}\left(|s_k|\,e^{-j\gamma_k}\right)\frac{\partial}{\partial\theta_i}\left(|s_k|\,e^{j\gamma_k}\right) - \left(\frac{\partial|s_k|}{\partial\theta_i}\right)^2 \tag{95}$$

$$= \left(\frac{\partial|s_k|}{\partial\theta_i}e^{-j\gamma_k} - js_k^*\frac{\partial\gamma_k}{\partial\theta_i}\right)\left(\frac{\partial|s_k|}{\partial\theta_i}e^{j\gamma_k} + js_k\frac{\partial\gamma_k}{\partial\theta_i}\right) - \left(\frac{\partial|s_k|}{\partial\theta_i}\right)^2 \tag{96}$$

$$= js_k\frac{\partial\gamma_k}{\partial\theta_i}\frac{\partial|s_k|}{\partial\theta_i}e^{-j\gamma_k} - js_k^*\frac{\partial\gamma_k}{\partial\theta_i}\frac{\partial|s_k|}{\partial\theta_i}e^{j\gamma_k} + |s_k|^2\left(\frac{\partial\gamma_k}{\partial\theta_i}\right)^2 \tag{97}$$

$$= 2\frac{\partial|s_k|}{\partial\theta_i}\frac{\partial\gamma_k}{\partial\theta_i}\mathrm{Re}\left\{js_ke^{-j\gamma_k}\right\} + |s_k|^2\left(\frac{\partial\gamma_k}{\partial\theta_i}\right)^2 \tag{98}$$

$$= 2\frac{\partial|s_k|}{\partial\theta_i}\frac{\partial\gamma_k}{\partial\theta_i}\mathrm{Re}\left\{j\,|s_k|\right\} + |s_k|^2\left(\frac{\partial\gamma_k}{\partial\theta_i}\right)^2 \tag{99}$$

$$= |s_k|^2\left(\frac{\partial\gamma_k}{\partial\theta_i}\right)^2 \tag{100}$$

and (69), (67) follows directly from (62). ∎

Appendix C
Proof of Theorem 2

Proof: With

$$s_k^*\frac{\partial}{\partial\phi}s_k = js_k^*s_k \quad \text{and} \quad s_k^*\frac{\partial}{\partial\Omega}s_k = jkT_ss_k^*s_k \tag{101}$$

(71), (72), and (74) follow directly from (66). Moreover, since no simple form could be found for the derivatives w.r.t. ϵ, (73) is obtained by directly applying (67). Furthermore, with (101) and (66) we obtain

$$\left[\tilde{\mathbf{F}}_{\mathbf{y}}\right]_{\epsilon\phi} = \frac{1}{\pi\left(N_0/T_s\right)}\sum_k \kappa_1\left(\frac{|s_k|^2}{N_0/T_s}\right)\mathrm{Im}\left\{s_k^*\frac{\partial}{\partial\epsilon}s_k\right\} \tag{102}$$

$$= \frac{1}{\pi\left(N_0/T_s\right)}\mathrm{Im}\left\{\sum_k \kappa_1\left(\frac{|s_k|^2}{N_0/T_s}\right)s_k^*\frac{\partial}{\partial\epsilon}s_k\right\} \tag{103}$$

$$= \frac{1}{\pi\left(N_0/T_s\right)}\mathrm{Im}\Bigg\{\sum_k \kappa_1\left(\frac{|s_k|^2}{N_0/T_s}\right)\sum_n\sum_m a_n^*a_m \times g\left(kT_s - nT - \epsilon T\right)\dot{g}\left(kT_s - mT - \epsilon T\right)\Bigg\} \tag{104}$$

$$\xrightarrow{p} \frac{1}{\pi\left(N_0/T_s\right)}\sum_k\sum_n\sum_m \mathrm{E}\left[\kappa_1\left(\frac{|s_k|^2}{N_0/T_s}\right)\mathrm{Im}\left\{a_n^*a_m\right\}\right] \times g\left(kT_s - nT - \epsilon T\right)\dot{g}\left(kT_s - nT - \epsilon T\right) \tag{105}$$

$$= 0, \tag{106}$$

where (105) is due to the law of large numbers and the assumption of i.i.d. symbols $\{a_n\}$, and $\dot{g}(\cdot)$ denotes the derivative w.r.t. time. Moreover, (106) is due to that fact that $g(t)$ is real

valued. Equivalently, with (101), (66), and i.i.d. symbols $\{a_n\}$ we obtain

$$\left[\tilde{\mathbf{F}}_{\mathbf{y}}\right]_{\epsilon\Omega} = \frac{1}{\pi\left(N_0/T_s\right)} \sum_k \kappa_1\left(\frac{|s_k|^2}{N_0/T_s}\right) kT_s \mathrm{Im}\left\{s_k^* \frac{\partial}{\partial \epsilon} s_k\right\} \quad (107)$$

$$\xrightarrow{p} 0, \quad (108)$$

by applying the same steps applied for $\left[\tilde{\mathbf{F}}_{\mathbf{y}}\right]_{\epsilon\phi}$. ∎

Appendix D
Proof of (79)

Before proving (79), we need to circumvent a technicality that arises because the proof is based on Jensen's inequality. As we assume that $g(t)$ is a strictly bandlimited pulse, it has an infinite time duration and thus we have to sum over $k \in (-\infty, \infty)$ to obtain the FI. However, Jensen's inequality does not hold for infinite measures, see, e.g., [38, Chapter 8.3] for a discussion on that matter. To circumvent this technicality, we exploit the fact that for large N the signal energy outside the data frame of length NT is vanishingly small compared to the signal energy inside the data frame. Furthermore, the signal carries the FI of its unknown parameters where its energy lies and thus we restrict the summation interval to $k \in [-K, K-1]$, where $K = \frac{1}{2}MN$, i.e., we only consider the part of the receive signal where the actual data symbols are. This allows us to obtain very tight bounds using Jensen's inequality. Moreover, the summation interval is chosen to be symmetric, since this maximizes the CRLB of Ω, as pointed out in [26, p. 334] and [39, p. 60]. Equipped with this discussion, we can now prove (79).

Proof: Due to (28) and (77) we know that the cross terms can be neglected and thus we only have to prove that

$$\left[\tilde{\mathbf{F}}_{\mathbf{y}}\right]_{\theta_i\theta_i} \leq \frac{1}{2\pi}\kappa_1\left(\frac{E_s}{N_0 M}\right)\left[\mathbf{F}_{\mathbf{r}}\right]_{\theta_i\theta_i}. \quad (109)$$

Let us start with (71)

$$\left[\tilde{\mathbf{F}}_{\mathbf{y}}\right]_{\phi\phi} = \frac{1}{\pi\left(N_0/T_s\right)} \sum_k \kappa_1\left(\frac{|s_k|^2}{N_0/T_s}\right)|s_k|^2 \quad (110)$$

$$= \frac{1}{\pi}\sum_k f\left(\frac{|s_k|^2}{N_0/T_s}\right) \quad (111)$$

$$\leq \frac{NM}{\pi} f\left(\frac{1}{NM(N_0/T_s)}\sum_k |s_k|^2\right) \quad (112)$$

$$= \frac{NM}{\pi} f\left(\frac{1}{2NM}\left[\mathbf{F}_{\mathbf{r}}\right]_{\phi\phi}\right) \quad (113)$$

$$= \frac{1}{2\pi}\kappa_1\left(\frac{E_s}{N_0 M}\right)\left[\mathbf{F}_{\mathbf{r}}\right]_{\phi\phi}, \quad (114)$$

where (112) is due to Jensen's inequality and the concavity of $f(x)$, which can be seen in Fig. 6a, and (113) and (114) are due to (9) and (10). Equivalently, for (72) we obtain

$$\left[\tilde{\mathbf{F}}_{\mathbf{y}}\right]_{\Omega\Omega} = \frac{1}{\pi\left(N_0/T_s\right)} \sum_k \kappa_1\left(\frac{|s_k|^2}{N_0/T_s}\right) k^2 T_s^2 |s_k|^2 \quad (115)$$

$$= \frac{1}{\pi}\sum_k f\left(\frac{|s_k|^2}{N_0/T_s}\right) k^2 T_s^2 \quad (116)$$

$$\leq \frac{1}{\pi} f\left(\frac{\sum_k k^2 T_s^2 |s_k|^2}{(N_0/T_s)\sum_k k^2 T_s^2}\right)\sum_k k^2 T_s^2 \quad (117)$$

$$= \frac{1}{\pi} f\left(\frac{[\mathbf{F}_{\mathbf{r}}]_{\Omega\Omega}}{2\sum_k k^2 T_s^2}\right)\sum_k k^2 T_s^2 \quad (118)$$

$$= \frac{1}{2\pi}\kappa_1\left(\frac{[\mathbf{F}_{\mathbf{r}}]_{\Omega\Omega}}{2\sum_k k^2 T_s^2}\right)[\mathbf{F}_{\mathbf{r}}]_{\Omega\Omega}, \quad (119)$$

where (117) is again due to Jensen's inequality and the concavity of $f(x)$, and (118) and (119) are due to (11) and (12). Using Faulhaber's formula and $K = \frac{1}{2}MN$, we obtain

$$\sum_{k=-K}^{K-1} k^2 = 2\sum_{k=1}^{K} k^2 - K^2 \quad (120)$$

$$= 2\frac{2K^3 + 3K^2 + K}{6} - K^2 \quad (121)$$

$$= \frac{M^3}{12}N^3 + \frac{M}{6}N. \quad (122)$$

Since we are interested in results for large N, we use (12) and (122) to compute the limit

$$\lim_{N\to\infty} \frac{[\mathbf{F}_{\mathbf{r}}]_{\Omega\Omega}}{2\sum_k k^2 T_s^2} = \frac{E_s}{N_0}\frac{T^2}{12}\frac{12}{T_s^2 M^3} \quad (123)$$

$$= \frac{E_s}{N_0 M}. \quad (124)$$

Thus, for $N \to \infty$ we obtain

$$\left[\tilde{\mathbf{F}}_{\mathbf{y}}\right]_{\Omega\Omega} \leq \frac{1}{2\pi}\kappa_1\left(\frac{E_s}{N_0 M}\right)\left[\mathbf{F}_{\mathbf{r}}\right]_{\Omega\Omega}. \quad (125)$$

Let us now turn to ϵ. As can be seen in Fig. 4, the CRLB, and thus the FI, is highly dependent on the true value of ϵ. However, we argued that if the oversampling factor M is an irrational number, this dependency will average out, i.e.,

$$\left[\tilde{\mathbf{F}}_{\mathbf{y}}\right]_{\epsilon\epsilon} \xrightarrow{p} \mathrm{E}_\epsilon\left[\left[\tilde{\mathbf{F}}_{\mathbf{y}}\right]_{\epsilon\epsilon}\right] \quad (126)$$

$$= \frac{1}{\pi\left(N_0/T_s\right)}\sum_k \int_{-0.5}^{0.5} \kappa_1\left(\frac{|s_k|^2}{N_0/T_s}\right)\frac{\partial}{\partial\epsilon}s_k^*\frac{\partial}{\partial\epsilon}s_k - \kappa_2\left(\frac{|s_k|^2}{N_0/T_s}\right)\left(\frac{\partial}{\partial\epsilon}|s_k|\right)^2 d\epsilon \quad (127)$$

$$= \frac{T^2}{\pi\left(N_0/T_s\right)}\frac{1}{T}\sum_k \int_{kT_s-0.5T}^{kT_s+0.5T} \kappa_1\left(\frac{|s(t)|^2}{N_0/T_s}\right)\frac{\partial}{\partial t}s^*(t)\frac{\partial}{\partial t}s(t) - \kappa_2\left(\frac{|s(t)|^2}{N_0/T_s}\right)\left(\frac{\partial}{\partial t}\sqrt{|s(t)|^2}\right)^2 dt, \quad (128)$$

where (128) is due to the substitution $t = kT_s - \epsilon T$. We observe that (128) is a sum of NM integrals, with the centers at kT_s and an interval length of T. Thus, the integrals overlap such that

$$\mathrm{E}_\epsilon\left[\left[\tilde{\mathbf{F}}_{\mathbf{y}}\right]_{\epsilon\epsilon}\right] = \frac{T^2}{\pi\left(N_0/T_s\right)}\frac{M}{T}\int_{-\frac{N}{2}T}^{\frac{N}{2}T}\kappa_1\left(\frac{|s(t)|^2}{N_0/T_s}\right)\frac{\partial}{\partial t}s^*(t)\frac{\partial}{\partial t}s(t) - \kappa_2\left(\frac{|s(t)|^2}{N_0/T_s}\right)\left(\frac{\partial}{\partial t}\sqrt{|s(t)|^2}\right)^2 dt. \tag{129}$$

With

$$\int_{-\frac{N}{2}T}^{\frac{N}{2}T}|s(t)|^2\,dt \approx \sum_n\sum_m a_n^* a_m\int_{-\infty}^{\infty} g^*\left(t-nT\right)g\left(t-mT\right)dt \tag{130}$$

$$\xrightarrow{p}\sum_n \mathrm{E}\left[|a_n|^2\right]\int_{-\infty}^{\infty}|g\left(t-nT\right)|^2\,dt \tag{131}$$

$$= NE_s \tag{132}$$

due to i.i.d. symbols we obtain

$$\begin{aligned}&\mathrm{E}_\epsilon\left[\left[\tilde{\mathbf{F}}_{\mathbf{y}}\right]_{\epsilon\epsilon}\right]\\ &\le \frac{T^2}{\pi\left(N_0/T_s\right)}\frac{M}{T}NT\\ &\quad\times\left[\kappa_1\left(\frac{\frac{1}{NT}\int_{-\frac{N}{2}T}^{\frac{N}{2}T}|s(t)|^2\,dt}{N_0/T_s}\right)\frac{1}{NT}\int_{-\frac{N}{2}T}^{\frac{N}{2}T}\frac{\partial}{\partial t}s^*(t)\frac{\partial}{\partial t}s(t)dt\right.\\ &\quad\left.-\kappa_2\left(\frac{\frac{1}{NT}\int_{-\frac{N}{2}T}^{\frac{N}{2}T}|s(t)|^2\,dt}{N_0/T_s}\right)\left(\frac{\partial}{\partial t}\sqrt{\frac{1}{NT}\int_{-\frac{N}{2}T}^{\frac{N}{2}T}|s(t)|^2\,dt}\right)^2\right]\end{aligned} \tag{133}$$

$$\begin{aligned}&\xrightarrow{p}\frac{T^2}{\pi\left(N_0/T_s\right)}\frac{M}{T}\kappa_1\left(\frac{E_s/T}{N_0/T_s}\right)\\ &\qquad\times\sum_n\mathrm{E}\left[|a_n|^2\right]\int_{-\frac{N}{2}T}^{\frac{N}{2}T}\left|\frac{\partial}{\partial t}g\left(t-nT\right)\right|^2 dt\end{aligned} \tag{134}$$

$$= \frac{1}{\pi}\kappa_1\left(\frac{E_s}{N_0M}\right)N\frac{E_s}{N_0}T^2 4\pi^2\frac{\int_{-\infty}^{\infty}f^2\,|G(f)|^2\,df}{\int_{-\infty}^{\infty}|G(f)|^2\,df} \tag{135}$$

$$= \frac{1}{2\pi}\kappa_1\left(\frac{E_s}{N_0M}\right)\left[\mathbf{F}_{\mathbf{r}}\right]_{\epsilon\epsilon}. \tag{136}$$

As the FI averaged over ϵ, i.e., the LHS of (133), is concave in the signal energy (see Fig. 5), the bounding (133) is similar to Jensen's inequality. However, since we integrate not only over $|s(t)|^2$ but also over $\frac{\partial}{\partial t}s^*(t)\frac{\partial}{\partial t}s(t) = \left|\frac{\partial}{\partial t}s(t)\right|^2$ (133) is not rigorously justified by Jensen's inequality. Thus, we performed simulations using raised cosine and root raised cosine filters $g(t)$ and found that we indeed obtain an upper bound on the FI and thus a lower bound on the CRLB. For a raised cosine pulse $g(t)$ with rolloff $\alpha = 0.2$ this can be seen in Fig. 5. Moreover, (134) is due to (132), (135) is proven in [26, p. 336], and the final result is due to (14). ∎

References

[1] B. Murmann, "Energy limits in a/d converters," in *Proc. IEEE Faibl. Tens. Faibl. Consomm.*, Paris, France, Jun. 2013.

[2] ——, "ADC performance survey 1997-2019." [Online]. Available: http://web.stanford.edu/ murmann/adcsurvey.html

[3] L. Landau, M. Dörpinghaus, and G. Fettweis, "1-bit quantization and oversampling at the receiver: Communication over bandlimited channels with noise," *IEEE Commun. Lett.*, vol. 21, no. 5, pp. 1007–1010, May 2017.

[4] L. Landau, M. Dörpinghaus, and G. P. Fettweis, "1-bit quantization and oversampling at the receiver: Sequence-based communication," *EURASIP J. Wirel. Commun. Netw.*, vol. 2018, Apr. 2018.

[5] S. Bender, M. Dörpinghaus, and G. Fettweis, "On the achievable rate of bandlimited continuous-time 1-bit quantized AWGN channels," in *Proc. IEEE Int. Symp. Inf. Theory*, Aachen, Germany, Jun. 2017, pp. 2083–2087.

[6] A. Gokceoglu, E. Bjornson, E. G. Larsson, and M. Valkama, "Spatio-temporal waveform design for multiuser massive MIMO downlink with 1-bit receivers," *IEEE J. Sel. Top. Signal Process.*, vol. 11, no. 2, pp. 347–362, Mar. 2017.

[7] A. B. Üçüncü and A. Ö. Yilmaz, "Oversampling in one-bit quantized massive MIMO systems and performance analysis," *IEEE Trans. Wirel. Commun.*, vol. 17, no. 12, pp. 7952–7964, 2018.

[8] Z. Shao, L. Landau, and R. C. de Lamare, "Study of channel estimation with oversampling for 1-bit large-scale MIMO systems," May 2019. [Online]. Available: http://arxiv.org/abs/1905.05319

[9] P. Neuhaus, M. Dörpinghaus, and G. Fettweis, "Oversampled 1-bit quantized wideband systems: Is it better to spend samples in time or in space?" in *Proc. IEEE Int. Work. Signal Process. Adv. Wirel. Commun.*, Cannes, France, Jul. 2019.

[10] D. Zhu, R. Bendlin, S. Akoum, A. Ghosh, and R. W. Heath, "Directional frame timing synchronization in wideband millimeter-wave systems with low-resolution ADCs," 2018. [Online]. Available: https://arxiv.org/abs/1809.02890

[11] ——, "Double-sequence frequency synchronization for wideband millimeter-wave systems with few-bit ADCs," Dec. 2018. [Online]. Available: http://arxiv.org/abs/1812.03629

[12] S. Jacobsson, C. Lindquist, G. Durisi, T. Eriksson, and C. Studer, "Timing and frequency synchronization for 1-bit massive MU-MIMO-OFDM downlink," May 2019. [Online]. Available: http://arxiv.org/abs/1905.07792

[13] A. Wadhwa and U. Madhow, "Near-coherent QPSK performance with coarse phase quantization: A feedback-based architecture for joint phase/frequency synchronization and demodulation," *IEEE Trans. Signal Process.*, vol. 64, no. 17, pp. 4432–4443, Sep. 2016.

[14] M. Schlüter, M. Dörpinghaus, and G. P. Fettweis, "On the timing synchronization under 1-bit quantization and oversampling," in *Proc. IEEE Stat. Signal Process. Work.*, Freiburg im Breisgau, Germany, Jun. 2018, pp. 198–202.

[15] ——, "Least squares phase estimation of 1-bit quantized signals with phase dithering," in *Proc. IEEE Int. Work. Signal Process. Adv. Wirel. Commun.*, Cannes, France, Jul. 2019.

[16] A. Genz and F. Bretz, *Computation of Multivariate Normal and t Probabilities*, 1st ed. Berlin Heidelberg: Springer, 2009.

[17] M. Stein, A. Mezghani, and J. A. Nossek, "A lower bound for the Fisher information measure," *IEEE Signal Process. Lett.*, vol. 21, no. 7, pp. 796–799, Jul. 2014.

[18] M. Stein, "Performance analysis for time-of-arrival estimation with oversampled low-complexity 1-bit A/D conversion," in *Proc. IEEE Int. Conf. Acoust. Speech Signal Process.*, New Orleans, USA, Mar. 2017, pp. 4491–4495.

[19] M. Schlüter, M. Dörpinghaus, and G. P. Fettweis, "Bounds on channel parameter estimation with 1-bit quantization and oversampling," in *Proc. IEEE Int. Work. Signal Process. Adv. Wirel. Commun.*, Kalamata, Greece, Jun. 2018.

[20] A. Mezghani, F. Antreich, and J. A. Nossek, "Multiple parameter estimation with quantized channel output," in *IEEE Int. ITG Work. Smart Antennas*, Bremen, Germany, Feb. 2010, pp. 143–150.

[21] M. Schlüter, M. Dörpinghaus, and G. Fettweis, "Bounds on phase and frequency estimation from 1-bit quantized signals with phase dithering," in *Proc. IEEE Int. Conf. Commun.*, Shanghai, China, May 2019.

[22] A. Wadhwa, U. Madhow, and N. R. Shanbhag, "Slicer architectures for analog-to-information conversion in channel equalizers," *IEEE Trans. Commun.*, vol. 65, no. 3, pp. 1234–1246, Mar. 2017.

[23] F. Neeser and J. Massey, "Proper complex random processes with applications to information theory," *IEEE Trans. Inf. Theory*, vol. 39, no. 4, pp. 1293–1302, Jul. 1993.

[24] H. Meyr, M. Oerder, and A. Polydoros, "On sampling rate, analog prefiltering, and sufficient statistics for digital receivers," *IEEE Trans. Commun.*, vol. 42, no. 12, pp. 3208–3214, 1994.

[25] G. Ascheid, M. Oerder, J. Stahl, and H. Meyr, “An all digital receiver architecture for bandwidth efficient transmission at high data rates,” *IEEE Trans. Commun.*, vol. 37, no. 8, pp. 804 – 813, 1989.

[26] H. Meyr, M. Moeneclaey, and S. Fechtel, *Digital Communication Receivers: Synchronization, Channel Estimation, and Signal Processing*. New York, NY, USA: John Wiley & Sons, Inc., 1997.

[27] R. A. Horn and C. R. Johnson, *Matrix analysis*, reprint. ed. Cambridge [u.a.]: Cambridge Univ. Press, 1999.

[28] J. M. Wooldridge, “Estimation and inference for dependent processes,” in *Handb. Econom. Vol. IV*. Amsterdam: Elsevier, 1994, ch. 45.

[29] H. C. Papadopoulos, G. W. Wornell, and A. V. Oppenheim, “Sequential signal encoding from noisy measurements using quantizers with dynamic bias control,” *IEEE Trans. Inf. Theory*, vol. 47, no. 3, pp. 978–1002, Mar. 2001.

[30] A. Host-Madsen and P. Handel, “Effects of sampling and quantization on single-tone frequency estimation,” *IEEE Trans. Signal Process.*, vol. 48, no. 3, pp. 650–662, Mar. 2000.

[31] K. Zografos and K. Ferentinos, “An information theoretic argument for the validity of the exponential model,” *Metrika*, vol. 41, no. 1, pp. 109–119, 1994.

[32] M. Stein, J. A. Nossek, and K. Barb, “Fisher information lower bounds with applications in hardware-aware nonlinear signal processing,” May 2018. [Online]. Available: https://arxiv.org/abs/1512.03473v2

[33] M. Stein and J. A. Nossek, “Will the 1-bit GNSS receiver prevail?” in *IEEE/ION Position, Locat. Navig. Symp.*, Monterey, CA, USA, May 2014, pp. 1033–1040.

[34] M. Stein, S. Theiler, and J. A. Nossek, “Overdemodulation for high-performance receivers with low-resolution ADC,” *IEEE Wirel. Commun. Lett.*, vol. 4, no. 2, pp. 169–172, Apr. 2015.

[35] R. Zamir, “A proof of the Fisher information inequality via a data processing argument,” *IEEE Trans. Inf. Theory*, vol. 44, no. 3, pp. 1246–1250, May 1998.

[36] F. W. Olver, D. W. Lozier, R. F. Boisvert, and C. W. Clark, *NIST Handbook of Mathematical Functions*, 1st ed. New York, NY, USA: Cambridge University Press, 2010.

[37] M. Stein, K. Barbé, and J. A. Nossek, “DOA parameter estimation with 1-bit quantization - bounds, methods and the exponential replacement,” in *Int. ITG Work. Smart Antennas*. VDE, 2016.

[38] B. Fristedt and L. Gray, *A modern approach to probability theory*. Boston: Birkhäuser, 1997.

[39] U. Mengali and A. N. D’Andrea, *Synchronization Techniques for Digital Receivers*. New York: Plenum Press, 1997.